# Functional Analysis of Cellulose and Xyloglucan in the Walls of Stomatal Guard Cells of Arabidopsis[1][OPEN]

**Yue Rui and Charles T. Anderson***

Department of Biology (Y.R., C.T.A.) and Center for Lignocellulose Structure and Formation (C.T.A.), Pennsylvania State University, University Park, Pennsylvania 16802

Stomatal guard cells are pairs of specialized epidermal cells that control water and $CO_2$ exchange between the plant and the environment. To fulfill the functions of stomatal opening and closure that are driven by changes in turgor pressure, guard cell walls must be both strong and flexible, but how the structure and dynamics of guard cell walls enable stomatal function remains poorly understood. To address this question, we applied cell biological and genetic analyses to investigate guard cell walls and their relationship to stomatal function in Arabidopsis (*Arabidopsis thaliana*). Using live-cell spinning disk confocal microscopy, we measured the motility of cellulose synthase (CESA)-containing complexes labeled by green fluorescent protein (GFP)-CESA3 and observed a reduced proportion of GFP-CESA3 particles colocalizing with microtubules upon stomatal closure. Imaging cellulose organization in guard cells revealed a relatively uniform distribution of cellulose in the open state and a more fibrillar pattern in the closed state, indicating that cellulose microfibrils undergo dynamic reorganization during stomatal movements. In *cesa3*$^{ie5}$ mutants defective in cellulose synthesis and *xxt1 xxt*2 mutants lacking the hemicellulose xyloglucan, stomatal apertures, changes in guard cell length, and cellulose reorganization were aberrant during fusicoccin-induced stomatal opening or abscisic acid-induced stomatal closure, indicating that sufficient cellulose and xyloglucan are required for normal guard cell dynamics. Together, these results provide new insights into how guard cell walls allow stomata to function as responsive mediators of gas exchange at the plant surface.

Stomata are pores with adjustable apertures that are present in the aerial tissues of vascular land plants. An individual stomatal pore is surrounded by a pair of guard cells, the repeatable expansion and contraction of which control transpiration and gas exchange between the plant and the environment. Stomatal development involves a series of cell divisions and cell identity transitions that are tightly regulated by both intrinsic and extrinsic factors (Casson and Hetherington, 2010). In Arabidopsis (*Arabidopsis thaliana*), the genetic and molecular mechanisms underlying stomatal development have been well characterized and include a suite of transcription factors and upstream receptor-like kinase-mediated signaling pathways (for review, see Bergmann and Sack, 2007; Pillitteri and Torii, 2012). Stomata are patterned such that they typically are not directly adjacent to one another in the epidermis, following the so-called one-cell-spacing rule (Larkin et al., 1997), which is thought to be functionally important, since guard cells in clustered stomata might mechanically hinder each other during stomatal opening or closing.

Stomatal movement is driven by changes in turgor pressure in guard cells and is the consequence of external and internal signals that are perceived and integrated by guard cells (Kollist et al., 2014). Blue light, red light, high humidity, and low $CO_2$ concentration induce the elevation of turgor pressure in guard cells, a process involving the activation of $H^+$-ATPases, which in turn triggers the uptake of ions such as $K^+$ and $Cl^-$ as well as the production of solutes such as malate (Kim et al., 2010), causing guard cell expansion and stomatal opening. A fungal toxin, fusicoccin (FC), can also induce stomatal opening by promoting proton export from guard cells (Zeiger, 1983). In contrast, darkness, high $CO_2$ levels, and abscisic acid (ABA) trigger stomatal closure, which is dependent on the efflux of solutes from guard cells and a resultant drop in turgor (Kim et al., 2010). During stomatal movements, guard cell volume can fluctuate by up to 40%, which is accompanied by alterations of cell surface area through membrane turnover rather than physical deformation of the plasma membrane (Franks et al., 2001; Shope et al., 2003; Li et al., 2010). It has been proposed that the coordination between guard cells and neighboring epidermal cells and the unique mechanical properties of guard cells, especially their walls, facilitate stomatal movements (Franks et al., 1998).

Plant cell walls, which are dynamic extracellular structures wherein cellulose microfibrils are embedded in a matrix of other carbohydrate polymers and

[1] This work was supported by the Department of Biology and the Pennsylvania State Institutes of Energy and the Environment, Pennsylvania State University, by a Huck Dissertation Research Award to Y.R., and by the U.S. Department of Energy, Office of Science, Basic Energy Sciences (grant no. DE–SC0001090).

* Address correspondence to cta3@psu.edu.

The author responsible for distribution of materials integral to the findings presented in this article in accordance with the policy described in the Instructions for Authors (www.plantphysiol.org) is: Charles T. Anderson (cta3@psu.edu).

Y.R. and C.T.A. designed the research; Y.R. performed the research and analyzed the data; Y.R. and C.T.A. wrote the article.

[OPEN] Articles can be viewed without a subscription.

www.plantphysiol.org/cgi/doi/10.1104/pp.15.01066

 

structural proteins (Somerville et al., 2004), have been studied extensively in elongating cells such as those in etiolated hypocotyls and roots (for review, see Cosgrove, 2005) and terminally differentiated cells such as those in xylem vessels and interfascicular fibers (for review, see Zhong et al., 2010), but they are not as well understood in stomatal guard cells. Cellulose microfibrils are partially crystalline nanostructures composed of parallel 1,4-$\beta$-linked glucan chains (Somerville, 2006). They provide tensile strength to the wall and are usually oriented transversely to the growth axis of elongating cells (Green, 1962). Cellulose is synthesized at the cell surface by cellulose synthesis complexes (CSCs), which are six-lobed rosettes localized at the plasma membrane (Kimura et al., 1999). Each lobe of a rosette is thought to contain multiple cellulose synthase (CESA) proteins, which constitute the catalytic machinery of CSCs. Live-cell imaging of fluorescent protein-tagged CESAs has demonstrated that cortical microtubules (MTs) dictate the trajectories of CSCs, which move bidirectionally with an average speed of approximately 330 nm $min^{-1}$ along linear tracks that are aligned with MTs (Paredez et al., 2006). However, the motility of CSCs is not strictly dependent on the presence of MTs (Paredez et al., 2006): lower MT abundance in Arabidopsis etiolated hypocotyl epidermal cells can result in a higher proportion of CSCs that track independently of MTs and an increase in CSC speed (Chen et al., 2010; Bischoff et al., 2011; Fujita et al., 2011), suggesting that CSCs might move faster in the absence of MT guidance. Despite these advances in our understanding of CSC behavior, CSC dynamics have not been reported in guard cells, and it also remains unknown whether CSC distribution, motility, and/or association with MTs are altered as stomata open or close, during which MTs in guard cell have been reported to undergo dynamic rearrangements and changes in abundance (Eisinger et al., 2012a, 2012b).

In Arabidopsis, the *CESA* gene family has 10 members (Richmond, 2000): *CESA1*, *CESA3*, *CESA6*, and *CESA6*-like (*CESA2*, *CESA5*, and *CESA9*) are involved in primary cell wall biosynthesis (Arioli et al., 1998; Fagard et al., 2000; Scheible et al., 2001), *CESA4*, *CESA7*, and *CESA8* are involved in secondary cell wall biosynthesis (Turner and Somerville, 1997; Taylor et al., 1999, 2003), and *CESA10* appears to function in the production of seed coat mucilage (Griffiths et al., 2015). Specifically for primary wall CSCs, biochemical and genetic studies have indicated that CESA1 and CESA3 are constitutive components of the CSC, whereas CESA6 and CESA6-like proteins have partially redundant functions and likely constitute a third catalytic component of the CSC (Desprez et al., 2007; Persson et al., 2007). Point mutations in these *CESA*s, such as *cesa1*$^{rsw1}$ (at a restrictive temperature), *cesa3*$^{eli1}$, and *cesa6*$^{prc1}$, lead to smaller seedlings and reduced cellulose content compared with wild-type controls (Arioli et al., 1998; Fagard et al., 2000; Caño-Delgado et al., 2003). However, whether these cellulose-deficient mutants have stomatal defects, and whether cellulose synthesis is indispensable for stomatal development and/or function, have not been reported. An Arabidopsis secondary wall *CESA* mutant, *cesa7*$^{irx3\text{-}5}$, displays reduced stomatal apertures, but this phenotype was attributed to smaller overall guard cell size and/or a defect in xylem function (Liang et al., 2010) rather than to a direct effect of cellulose deficiency in the guard cell wall.

To achieve rapid and reversible stomatal movements, the walls of guard cells must possess enough physical strength to withstand high turgor pressure and sufficient elasticity to expand and contract repetitively. Polarized light microscopy and field emission scanning electron microscopy have revealed that cellulose microfibrils are arranged radially relative to the stomatal pore in mature guard cells so as to constrain radial cell expansion (Palevitz and Hepler, 1976; Fujita and Wasteneys, 2014), instead favoring longitudinal cell expansion during stomatal opening (Wu et al., 1985; Meckel et al., 2007). However, fundamental questions remain to be addressed, such as whether there are any differences in cellulose organization between open and closed stomatal guard cells, and if so, how cellulose reorientation and/or reorganization facilitate stomatal movements. Wall matrix polysaccharides, including hemicelluloses (e.g. xyloglucan) and pectins, are thought to interact with cellulose microfibrils (Somerville et al., 2004; Cosgrove, 2005) and are proposed to contribute to the anisotropic expansion of guard cell walls during stomatal movements (Wu et al., 1985). Immunolabeling using wall epitope-directed antibodies has detected the presence of xyloglucan and pectins in sugar beet (*Beta vulgaris*) guard cells (Majewska-Sawka et al., 2002). Pectic arabinans, in particular, have been demonstrated to be essential for FC-induced stomatal opening and ABA-induced stomatal closure, given that arabinanase digestion of epidermal peels prior to FC or ABA treatment impedes stomatal movements in several species (Jones et al., 2003, 2005). However, genetic evidence for the importance of matrix polysaccharides in stomatal function is still lacking.

In this study, we recorded and compared CSC dynamics, colocalization between CSCs and MTs, and cellulose organization in open versus closed stomatal guard cells in wild-type and mutant Arabidopsis plants. We found an increase in CSC speed and a reduced proportion of CSCs colocalizing with MTs as stomata close. By measuring stomatal aperture changes in the guard cells of two cell wall mutants, we determined that normal levels of cellulose and xyloglucan in guard cell walls are required to control stomatal aperture. We also observed that cellulose microfibrils display a relatively uniform distribution in open stomatal guard cells but a more fibrillar pattern in closed stomatal guard cells, indicating that cellulose is reorganized during stomatal movements.

## RESULTS

### GFP-CESA3 Particle Speed Increases upon Treatments That Induce Stomatal Closure

To investigate CSC activity in stomatal guard cells and test whether it varies in open versus closed

stomata, we measured CSC density and speed in stomatal guard cells from 6-d-old seedlings expressing GFP-CESA3 in the *cesa3*$^{je5}$ mutant background (Desprez et al., 2007) using time-lapse live-cell imaging. Young seedlings were used in this experiment because preliminary analyses demonstrated that there is a dramatic reduction in fluorescent protein (FP)-CESA1/3/6 particle density $\mu m^{-2}$ in guard cells from 1 to 2 weeks after germination (Supplemental Fig. S1). To validate that stomatal guard cells from young seedlings respond to ABA and dark treatments, which are normally used to induce stomatal closure in mature leaves, we carried out stomatal closure assays in 6-d-old seedlings expressing GFP-CESA3 and visualized stomatal apertures by staining with propidium iodide (PI), a fluorescent dye that highlights cell outlines. ABA or dark treatment for 2.5 h led to a significant decrease in average stomatal aperture compared with control conditions (Supplemental Fig. S2, A–F), suggesting that stomatal guard cells are functional in young tissues. To further test whether there is any difference in the kinetics of stomatal movement in younger versus older stomata, we performed time-course ABA and FC treatments to compare stomatal responses between 1- and 2-week-old seedlings. Stomata from 1-week-old seedlings displayed a gradual decrease or increase in aperture in response to ABA or FC, a trend similar to what was seen in stomata from 2-week-old seedlings, although the latter had a sharper aperture change during the first 0.5 h in ABA treatment or the first 1 h of FC treatment and larger aperture values at the end of FC treatment (Supplemental Fig. S2, G and H).

We first analyzed GFP-CESA3 particle density and speed in response to ABA treatment, which induces stomatal closure. Time average projections of GFP-CESA3 movement revealed a radial distribution of particle tracks that fan out from the stomatal pore (Fig. 1A), a pattern consistent with the radial organization of cortical MTs and the orientation of cellulose microfibrils reported previously in mature Arabidopsis guard cells (Lucas et al., 2006; Fujita and Wasteneys, 2014). Stomatal closure induced by ABA treatment for 2.5 h resulted in a slight but not significant decrease in GFP-CESA3 particle density in guard cells (Fig. 1A; 0.38 ± 0.03 [SE] particles $\mu m^{-2}$ in the absence of ABA versus 0.33 ± 0.03 particles $\mu m^{-2}$ in the presence of ABA; $n \geq 26$ guard cell pairs from at least nine seedlings, three independent experiments; $P = 0.2$, Student's $t$ test). However, the addition of ABA significantly sped up GFP-CESA3 particle movement by approximately 10% (Fig. 1B; Supplemental Movies S1 and S2). To examine whether the above trends in GFP-CESA3 behavior hold true in neighboring pavement cells, we performed similar analyses for pavement cells using the same image collections and found that ABA treatment also resulted in an insignificant change in GFP-CESA3 particle density but a significant increase in GFP-CESA3 particle motility in neighboring pavement cells (Supplemental Fig. S3).

To further test whether there is an increase in CSC motility in closed stomatal guard cells, we used dark treatment for 2.5 h to induce stomatal closure. Closed stomatal guard cells under this condition did not show any significant change in GFP-CESA3 particle density as compared with open stomatal guard cells (Fig. 1C; 0.27 ± 0.03 particles $\mu m^{-2}$ under the light control condition versus 0.35 ± 0.04 particles $\mu m^{-2}$ after dark treatment for 2.5 h; $n \geq 20$ guard cell pairs from at least nine seedlings, three independent experiments; $P = 0.1$, Student's $t$ test); however, average GFP-CESA3 particle speed was significantly higher relative to the light control condition (Fig. 1D; Supplemental Movies S3 and S4). Identical measurements of CSC activity were likewise conducted in neighboring pavement cells after a 2.5-h dark treatment, which also resulted in no significant change in GFP-CESA3 particle density but a significant increase in GFP-CESA3 particle speed compared with light controls (Supplemental Fig. S4). To address the possibility that exogenously supplied Suc might affect substrate availability during cellulose biosynthesis, and thus CSC activity, we also grew seedlings on plates lacking Suc and induced stomatal closure by dark treatment for 2.5 h. Again, there was no significant change in GFP-CESA3 particle density between the dark treatment and the light control condition in either guard cells (0.3 ± 0.03 particles $\mu m^{-2}$ under the light control condition versus 0.36 ± 0.02 particles $\mu m^{-2}$ after dark treatment for 2.5 h; $n \geq 26$ guard cell pairs from at least 10 seedlings, three independent experiments; $P = 0.1$, Student's $t$ test) or neighboring pavement cells (0.25 ± 0.03 particles $\mu m^{-2}$ under the light control condition versus 0.18 ± 0.03 particles $\mu m^{-2}$ after dark treatment for 2.5 h; $n \geq 16$ pavement cells from at least nine seedlings, three independent experiments; $P = 0.1$, Student's $t$ test). However, GFP-CESA3 particle movement was significantly faster after a 2.5-h dark treatment in both guard cells (234 ± 4 nm $min^{-1}$ under the light control condition versus 250 ± 5 nm $min^{-1}$ after dark treatment for 2.5 h; $n > 960$ particles out of more than 26 guard cell pairs from at least 10 seedlings per treatment, three independent experiments; $P < 0.02$, Student's $t$ test) and neighboring pavement cells (229 ± 3 nm $min^{-1}$ under the light control condition versus 263 ± 5 nm $min^{-1}$ after dark treatment for 2.5 h; $n > 930$ particles out of more than 16 guard cell pairs from at least nine seedlings per treatment, three independent experiments; $P < 0.001$, Student's $t$ test). Taken together, these results indicate that ABA and dark treatments lead to increased CSC motility in both stomatal guard cells and neighboring pavement cells.

### Colocalization between GFP-CESA3 Particles and Microtubules Is Reduced in Guard Cells upon Stomatal Closure

Since CSCs move in alignment with cortical MTs (Paredez et al., 2006) and MT organization changes as stomata close in Arabidopsis guard cells (Eisinger et al., 2012a, 2012b), we next asked whether CSCs might dissociate from underlying MTs and go off the rails

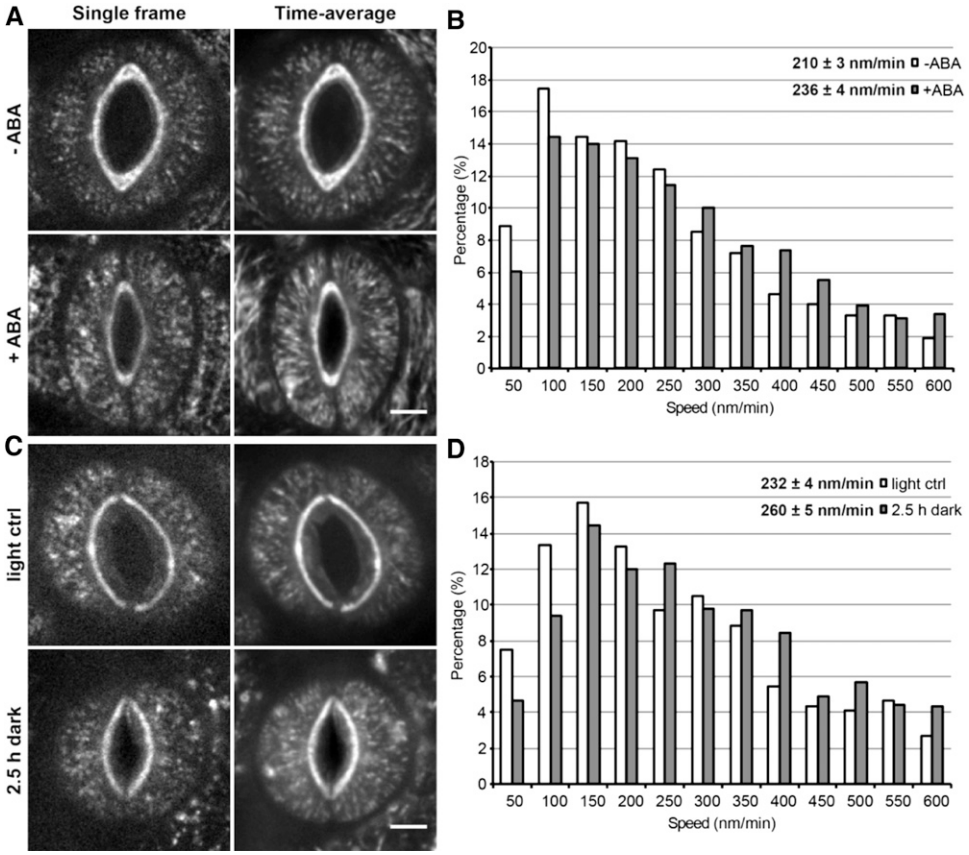


**Figure 1.** GFP-CESA3 particle motility increases in stomatal guard cells induced to close by ABA or dark treatment. A, Distribution of GFP-CESA3 particles and tracks in open or closed stomatal guard cells of 6-d-old seedlings in the absence or presence of 50 $\mu$M ABA, respectively. Single-frame images are on the left, and time average projections of 31 frames (10-s interval, 5-min total duration) are on the right. Bar = 5 $\mu$m. B, Histogram of GFP-CESA3 particle speed distributions ($n > 1{,}250$ particles in more than 26 guard cell pairs from at least nine seedlings per treatment, three independent experiments; $P < 0.01$, Student's $t$ test). C, Distribution of GFP-CESA3 particles and tracks in open or closed stomatal guard cells of 6-d-old seedlings grown on one-half-strength Murashige and Skoog (MS) + 1% Suc plates under light control or 2.5-h dark conditions, respectively. Single-frame images are on the left, and time average projections of 31 frames (10-s interval, 5-min total duration) are on the right. Bar = 5 $\mu$m. D, Histogram of GFP-CESA3 particle speed distributions ($n > 1{,}000$ particles in more than 20 guard cell pairs from at least nine seedlings per treatment, three independent experiments; $P < 0.01$, Student's $t$ test).

during stomatal closure. We performed dual-channel spinning disk confocal imaging of CESAs and MTs in guard cells using Arabidopsis 6-d-old seedlings expressing GFP-CESA3, a marker for CSCs, and mCherry-TUA5, a marker for MTs (Gutierrez et al., 2009), which allowed us to analyze colocalization between CSCs and MTs in guard cells at different developmental stages and functional states. An interesting finding in young guard cells was that CSCs and MTs are highly colocalized at the center of a guard cell pair (Fig. 2, A–C). Such colocalization might represent the aftereffects of cytokinesis in guard mother cells, during which the newly formed ventral cell wall of each guard cell must be reinforced. To compare the degree of CSC-MT colocalization between open and partially closed stomatal guard cells, we applied a 30-min dark treatment to induce stomatal closure. In both open and partially closed states, MTs in guard cells displayed the typical radial array (Fig. 2, E and H) and some CESA3 particles were distributed along MTs (Fig. 2, F and I). To quantify the degree of CSC-MT colocalization, we applied background subtraction and contrast enhancement to all of the images under the same parameters in ImageJ, used the software package Imaris (Bitplane) to automatically detect GFP-CESA3 particles, and scored particle colocalization with MTs in guard cells from which the autofluorescent phenolic ester rings had been cropped (Fig. 2, J and K), since this autofluorescence resulted in false-positive particle detection. Dark treatment for 30 min did not result in a significant change in GFP-CESA3 particle density in guard cells compared with the light control condition ($P = 0.06$, Student's $t$ test; Supplemental Table S1). However, guard cells exposed to the dark for 30 min were found to have a significantly lower percentage of GFP-CESA3 particles overlying MTs (median, 17.1%) than guard cells kept in the light (median, 22%; Fig. 2L). To investigate whether such a decrease in CSC-MT colocalization is simply due

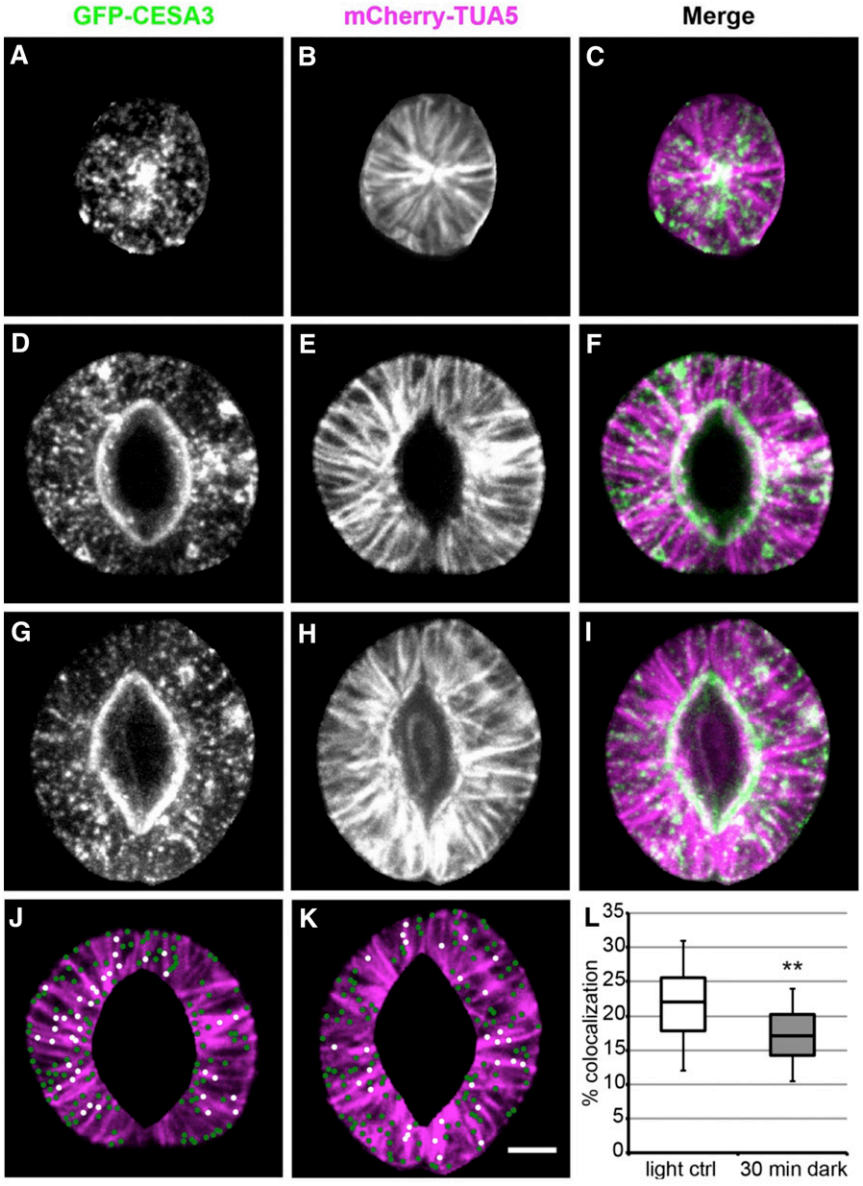


**Figure 2.** Colocalization of GFP-CESA3 particles and MTs decreases in guard cells upon stomatal closure. A to I, Maximum projections of z-series of GFP-CESA3 particles and mCherry-TUA5-labeled MTs in a young guard cell pair (A–C), guard cells with an open stoma (D–F) under light control conditions, and guard cells with a closed stoma (G–I) induced by dark treatment for 30 min. In all merged images on the right (C, F, and I), GFP-CESA3 labeling is in green and mCherry-TUA5 labeling is in magenta. J and K, Representations (dots) of GFP-CESA3 particles detected in the same guard cell pairs as in F and I, respectively, after cropping phenolic ester rings. Particles coaligned with MTs are represented as white dots, and those not colocalized with MTs are represented as green dots. Bar = 5 $\mu$m. L, Box plot of the percentage of GFP-CESA3 particles colocalized with MTs in guard cells under light control (ctrl) or 30-min dark conditions. Asterisks indicate a significant difference between treatments ($n > 3{,}000$ particles from more than 24 guard cell pairs for each treatment, more than three independent experiments; **, $P < 0.01$, Student's $t$ test).

to a decrease in MT abundance as stomata close, we applied autothresholding to the mCherry-TUA5 fluorescent images in ImageJ and quantified mCherry-TUA5 fluorescence area and intensity in guard cells. Dark treatment for 30 min did not lead to any significant change in guard cell area ($P = 0.07$, Student's $t$ test), the ratio of thresholded area to guard cell area ($P = 0.09$, Student's $t$ test), or mCherry-TUA5 fluorescence intensity ($P = 0.51$, Student's $t$ test) compared with the light control condition (Supplemental Table S1). These data rule out the possibility that less GFP-CESA3 particle density or loss of MTs is the cause for the reduced proportion of CSCs colocalizing with MTs in partially closed guard cells after dark treatment for 30 min.

To test whether the difference in the degree of CSC-MT colocalization is specific to stomatal guard cells, similar assessments of colocalization were performed using the same set of images but analyzing neighboring pavement cells as regions of interest (ROIs). Compared with light controls, exposure to the dark for 30 min did not lead to a significant change in the degree of colocalization between GFP-CESA3 particles and MTs in pavement cells (28.3% [median] for the light control versus 26.4% [median] for the 30-min dark treatment; Supplemental Fig. S5), and the average values under both conditions were higher than their respective counterparts in guard cells (30.7% ± 1.9% for pavement cells versus 21.8% ± 1% for guard cells under the light control condition, and 27.1% ± 1.2% for pavement cells versus 17.2% ± 0.9% for guard cells after the 30-min dark treatment). Together, these results suggest that, as stomata close in response to a dark stimulus, there is less coalignment between CSCs and MTs specifically in guard cells.

### Stomatal Aperture Is Correlated with the Amount of Cellulose Present in Guard Cells

As an initial test of whether cellulose is essential for stomatal function, we measured stomatal apertures in three mutants of primary wall-associated CESAs: *cesa3*$^{je5}$ (Desprez et al., 2007; Feraru et al., 2011), *cesa3*$^{eli1\text{-}1}$ (Caño-Delgado et al., 2003; Pysh et al., 2012), and *cesa6*$^{prc1\text{-}1}$ (Desnos et al., 1996; Fagard et al., 2000; MacKinnon et al., 2006). Stomatal apertures (for measurement legend in a stomatal complex, see Supplemental Fig. S6) were measured in rosette leaves from approximately 3-week-old plants after light treatment for 2.5 h. Among all three *cesa* mutants, only *cesa3*$^{je5}$ exhibited significantly larger stomatal apertures than wild-type controls (Fig. 3A). To investigate the reason for this difference among *cesa* alleles, we first measured cellulose content in whole rosette leaves of these mutants by the Updegraff method (Updegraff, 1969) and found that *cesa3*$^{je5}$ mutants had the most severe reduction in cellulose (Fig. 3B), suggesting that the larger stomatal apertures in *cesa3*$^{je5}$ mutants might be due to insufficient cellulose levels.

In addition to guard cells, many other cell types are present in whole rosette leaves; thus, to analyze cellulose content specifically in guard cells, we applied two independent imaging techniques. Pontamine Fast Scarlet 4B (S4B) is a fluorescent dye that specifically binds to cellulose (Anderson et al., 2010). Using rosette leaves from 3- to 4-week-old plants, we developed a staining protocol to facilitate penetration of the dye through the thick guard cell cuticle (see "Materials and Methods") and quantified fluorescence intensity in guard cells as an estimate of cellulose content (Supplemental Fig. S7A). Consistent with the Updegraff results in rosette leaves (Fig. 3B), *cesa3*$^{je5}$ guard cells also had the lowest S4B fluorescence intensity among the three *cesa* mutants (Fig. 3C; Supplemental Fig. S7A), resulting in a Pearson correlation coefficient of $-0.97$ between stomatal aperture and S4B fluorescence intensity ($P = 0.03$) and 0.85 between Updegraff quantification and S4B fluorescence intensity ($P = 0.15$). We also labeled cellulose in guard cells using CARBOHYDRATE-BINDING MODULE3a (CBM3a; Blake et al., 2006; Supplemental Fig. S7B) and measured fluorescence intensity. Similar to the S4B staining results, *cesa3*$^{je5}$ guard cells displayed lower CBM3a-associated fluorescence intensity than the other two *cesa* mutants, although this difference was not statistically significant (Fig. 3D). Together, these data suggest that there is a correlation between stomatal aperture and cellulose content in guard cells.

### *cesa3*$^{je5}$ Mutants Display Larger Stomatal Apertures, and GFP-CESA3 Expression Rescues This Phenotype

We next focused on *cesa3*$^{je5}$ mutants and first examined stomatal patterning on the abaxial side of 6-d-old *cesa3*$^{je5}$ cotyledons by PI staining. Compared with wild-type controls, in which stomata generally follow the one-cell-spacing rule (Bergmann and Sack, 2007), *cesa3*$^{je5}$ mutants displayed a significantly higher percentage of aberrantly adjacent pairs of stomata (15.6% ± 1.2% for *cesa3*$^{je5}$ versus 5.2% ± 0.1% for Col-0; $n > 450$ stomata from 18 seedlings per genotype, three independent experiments; $P < 0.01$, $\chi^2$ test; Supplemental Fig. S8). No stomatal trios, quartets, or clusters of more than four adjacent stomata were found in *cesa3*$^{je5}$ mutants. Together, these data suggest that *CESA3*, and potentially sufficient cellulose production, contribute to maintaining the normal developmental patterning and size of stomata. For subsequent experiments, we analyzed only single stomates in all genotypes.

When grown in soil, 3-week-old *cesa3*$^{je5}$ plants had significantly smaller rosettes with an approximately 33.3% decrease in diameter (Supplemental Fig. S9, A and B), delayed rosette leaf emergence, and smaller individual leaves (Supplemental Fig. S9C) compared with wild-type controls. We next tested stomatal responses to FC-induced stomatal opening at different time points in Col-0 and *cesa3*$^{je5}$ rosette leaves, measuring stomatal apertures every 0.5 h after adding 1 $\mu$M FC. During the 2.5-h FC treatment, Col-0 controls showed an almost linear increase in stomatal aperture from 0.6 ± 0 $\mu$m at 0 h to 2.7 ± 0.1 $\mu$m at 2.5 h, whereas *cesa3*$^{je5}$ mutants displayed a similar trend of increasing stomatal aperture, but with significantly larger average aperture (1.4 ± 0.1 $\mu$m at 0 h to 3.9 ± 0.1 $\mu$m at 2.5 h) than Col-0 controls at all time points (Fig. 4A). These numbers represent a 332.4% increase in average stomatal aperture in Col-0 plants but only a 181.3% increase in average stomatal aperture in *cesa3*$^{je5}$ plants as a result of FC treatment.

We likewise tested stomatal responses to ABA-induced closure in Col-0 and *cesa3*$^{je5}$ plants. Over the 2.5-h course of 50 $\mu$M ABA treatment, Col-0 controls exhibited a smooth decline in stomatal aperture from 3.3 ± 0.1 $\mu$m at 0 h to 0.6 ± 0 $\mu$m at 2.5 h; *cesa3*$^{je5}$ mutants also displayed a similar overall trend of stomatal aperture reduction, but with significantly larger apertures (4.2 ± 0.1 $\mu$m at 0 h to 1.5 ± 0.1 $\mu$m at 2.5 h) than wild-type controls at all time points (Fig. 4B). These values represent an 80.6% decrease in aperture in Col-0 stomata and a 63.8% decrease in aperture in *cesa3*$^{je5}$ stomata in response to ABA treatment.

Intrigued by the larger stomatal apertures in *cesa3*$^{je5}$ mutants, we next measured a suite of parameters (for measurement legend in a stomatal complex, see Supplemental Fig. S6) to test possible reasons for this phenotype. Factors contributing to stomatal aperture include (1) pore geometry, a component of which is pore length, (2) the overall dimensions of a guard cell pair (guard cell pair height and guard cell pair width), and (3) the geometry of a single guard cell (guard cell diameter and guard cell length, changes in which can be attributed to wall extensibility in the radial and longitudinal directions, respectively). Note that these parameters are geometrically correlated but distinct from one another. For example, in a stomatal complex, guard cell pair width is the sum of stomatal aperture plus the diameters of the two paired guard cells.

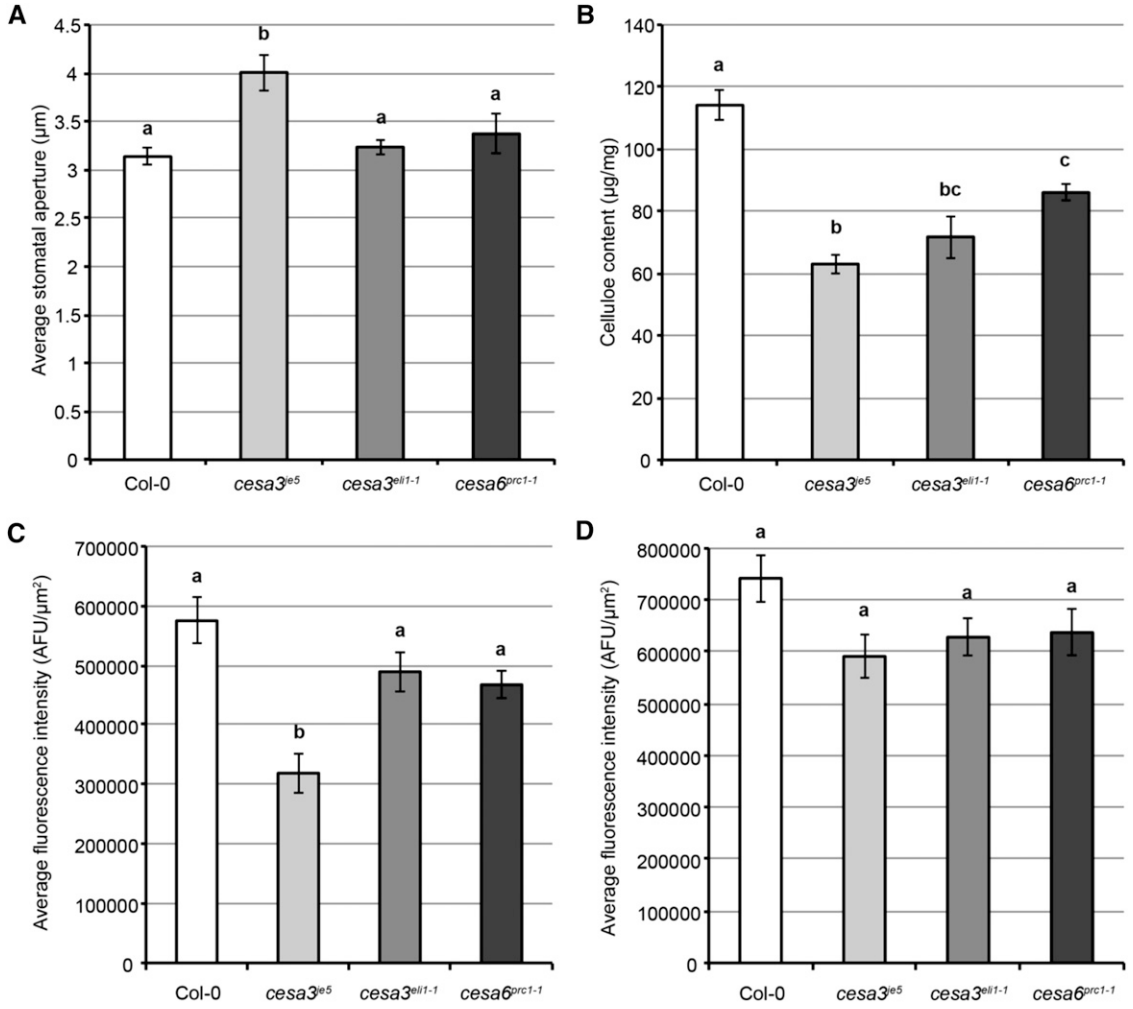


**Figure 3.** Larger stomatal aperture is correlated with more severe cellulose deficiency in guard cells. A, Average stomatal apertures in approximately 3-week-old rosette leaves of Columbia-0 (Col-0), *cesa3*$^{je5}$, *cesa3*$^{eli1-1}$, and *cesa6*$^{prc1-1}$ after light treatment for 2.5 h. Error bars indicate SE, and lowercase letters represent significantly different groups ($n \geq 40$ guard cell pairs per genotype; $P < 0.05$, one-way ANOVA and Tukey's test). B, Cellulose content measurements by the Updegraff method in 23-d-old rosette leaves of Col-0, *cesa3*$^{je5}$, *cesa3*$^{eli1-1}$, and *cesa6*$^{prc1-1}$. Error bars indicate SE, and lowercase letters represent significantly different groups ($n \geq 9$ technical replicates from two biological replicates; $P < 0.05$, one-way ANOVA and Tukey's test). C, Quantifications of S4B fluorescence intensity in guard cells of Col-0, *cesa3*$^{je5}$, *cesa3*$^{eli1-1}$, and *cesa6*$^{prc1-1}$. Error bars indicate SE, and lowercase letters represent significantly different groups ($n \geq 69$ guard cells per genotype; $P < 0.05$, one-way ANOVA and Tukey's test). D, Quantifications of CBM3a immunolabeling fluorescence intensity in guard cells of Col-0, *cesa3*$^{je5}$, *cesa3*$^{eli1-1}$, and *cesa6*$^{prc1-1}$. Error bars indicate SE, and lowercase letters represent significantly different groups ($n \geq 30$ guard cells per genotype; $P < 0.05$, one-way ANOVA and Tukey's test). AFU, Arbitrary fluorescence units.

Because overall stomatal pore size affects stomatal aperture, we measured pore length (for measurement legend in a stomatal complex, see Supplemental Fig. S6) and the ratio of stomatal aperture to pore length on a single stomate basis in Col-0 and *cesa3*$^{je5}$ stomata. If larger stomatal apertures stem simply from larger overall pore sizes, one would expect to see the same ratio of aperture to pore length in *cesa3*$^{je5}$ mutants and Col-0 controls. However, *cesa3*$^{je5}$ stomatal pores consistently had a higher ratio of aperture to pore length than Col-0 controls at the beginning or the end of the 2.5-h FC or ABA treatment (Table I), indicating that the larger stomatal aperture seen in *cesa3*$^{je5}$ mutants is likely due to factors other than a simple increase in pore size.

To test whether overall guard cell pair size is altered in *cesa3*$^{je5}$ plants, which could also contribute to larger stomatal aperture, we measured the heights and widths of guard cell pairs (for measurement legend in a stomatal complex, see Supplemental Fig. S6) at the beginning and the end of the 2.5-h FC or ABA treatment in Col-0 and *cesa3*$^{je5}$ mutants. Although a clear pattern in guard cell pair height was not evident from the measurements, *cesa3*$^{je5}$ mutants were consistently found to have significantly larger guard cell pair widths than wild-type guard cell pairs (Table I), resulting in smaller aspect ratios

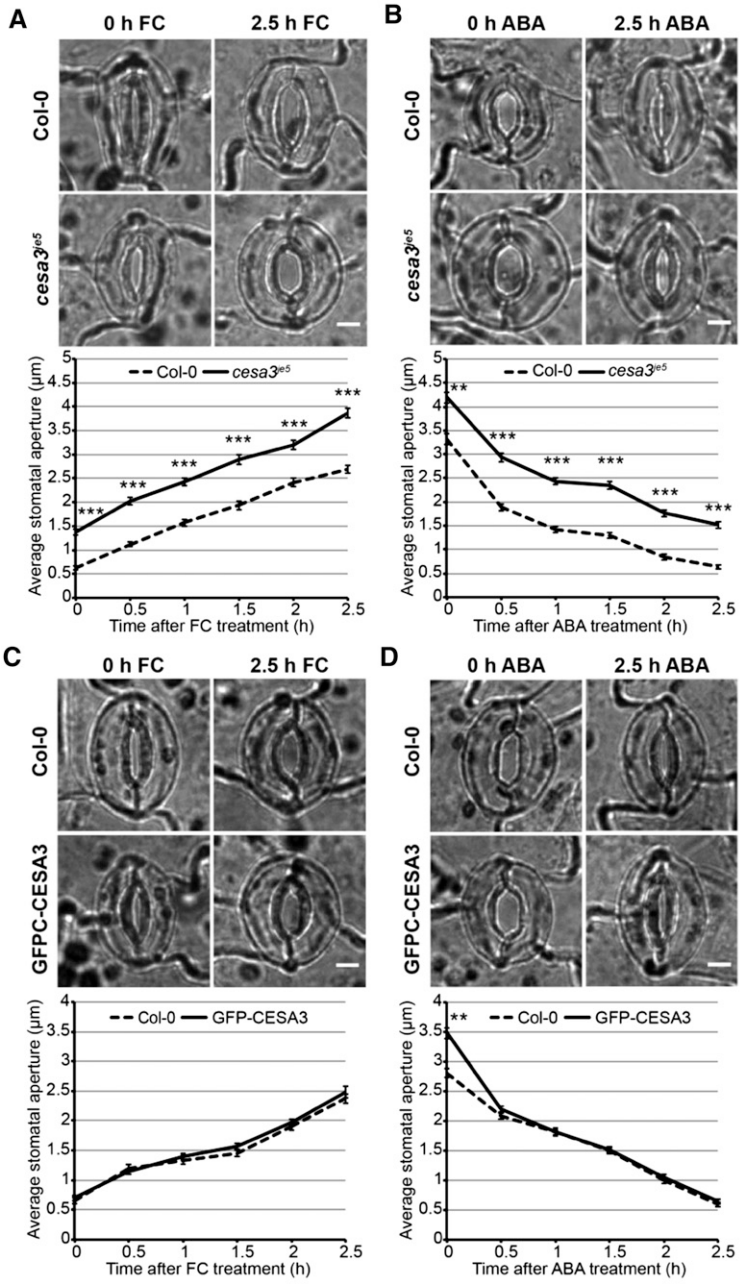


**Figure 4.** *cesa3*$^{je5}$ mutants exhibit larger stomatal apertures during FC or ABA treatment, and GFP-CESA3 expression largely complements these phenotypes. A and C, Stomatal responses to 1 $\mu$M FC-induced opening in epidermal peels of Col-0 and *cesa3*$^{je5}$ plants (A) and in epidermal peels of Col-0 and GFP-CESA3 transgenic plants (C), with representative bright-field stomatal images at the top and measurements of stomatal apertures at the bottom. Error bars indicate SE. Asterisks indicate significant differences between genotypes at each time point examined ($n \geq 100$ stomata per genotype per time point from three independent experiments; ***, $P < 0.001$, Student's *t* test). Bars = 5 $\mu$m. B and D, Stomatal responses to 50 $\mu$M ABA-induced closure in epidermal peels of Col-0 and *cesa3*$^{je5}$ plants (B) and in epidermal peels of Col-0 and GFP-CESA3 transgenic plants (D), with representative bright-field stomatal images at the top and measurements of stomatal apertures at different time points at the bottom. Error bars indicate SE. Asterisks indicate significant differences between genotypes at each time point examined ($n \geq 80$ stomata per genotype per time point from three independent experiments; **, $P < 0.01$ and ***, $P < 0.001$, Student's *t* test). Bars = 5 $\mu$m.

(Table I). Reasoning that the larger stomatal aperture phenotype we observed might be due to the increased guard cell pair width observed in *cesa3*$^{je5}$ mutants (Table I), we next analyzed the ratio of stomatal aperture to overall guard cell pair width on a single stomate basis. If larger stomatal aperture results simply from increased guard cell pair width, one would expect *cesa3*$^{je5}$ mutants to have the same ratio of stomatal aperture to guard cell pair width as Col-0 controls. However, compared with wild-type controls, *cesa3*$^{je5}$ mutants still had a

**Table I.** *Stomatal pore dimensions, guard cell pair dimensions, and guard cell dimensions in wild-type and cesa3$^{je5}$ mutant plants during FC or ABA treatment*

Stomatal aperture, stomatal pore length, ratio of aperture to pore length, guard cell pair height, guard cell pair width, aspect ratio of guard cell pairs (height to width), ratio of aperture to guard cell pair width, guard cell diameter, and guard cell length were measured on a single stomate basis using epidermal peels from 3- to 4-week-old plants. Values are presented as means ± SE ($n >$ 80 stomata for each genotype at each time point from three experiments). Lowercase letters represent significantly different groups ($P < 0.05$, one-way ANOVA and Tukey's test). ANOVA was performed within each treatment. NA, Not applicable.

| Treatment | Time after Treatment | Genotype | Average Stomatal Aperture | Average Stomatal Pore Length | Average Ratio of Aperture to Pore Length | Average Guard Cell Pair Height | Average Guard Cell Pair Width | Average Aspect Ratio of Guard Cell Pairs | Average Ratio of Aperture to Guard Cell Pair Width | Average Guard Cell Diameter | Average Guard Cell Length | Change in Average Guard Cell Length |
|---|---|---|---|---|---|---|---|---|---|---|---|---|
| | *h* | | *μm* | | | *μm* | | | | *μm* | | |
| FC | 0 | Col-0 | 0.6 ± 0.0 a | 10.3 ± 0.2 a,b | 0.05 ± 0.00 a | 26.0 ± 0.3 a | 17.1 ± 0.1 a | 1.53 ± 0.02 a | 0.03 ± 0.00 a | 7.3 ± 0.1 a | 24.9 ± 0.2 a | NA |
| | | *cesa3$^{je5}$* | 1.4 ± 0.1 c | 7.9 ± 0.1 c | 0.16 ± 0.01 b | 23.1 ± 0.2 c | 18.4 ± 0.1 c | 1.26 ± 0.01 b | 0.08 ± 0.00 c | 7.6 ± 0.1 b | 24.0 ± 0.1 b | NA |
| | 2.5 | Col-0 | 2.7 ± 0.1 b | 10.5 ± 0.2 a | 0.26 ± 0.01 c | 24.6 ± 0.3 b | 19.7 ± 0.2 b | 1.26 ± 0.01 b | 0.13 ± 0.00 b | 7.4 ± 0.1 a,b | 25.6 ± 0.3 a | 0.7 |
| | | *cesa3$^{je5}$* | 3.9 ± 0.1 d | 9.8 ± 0.1 b | 0.41 ± 0.01 d | 24.7 ± 0.2 b | 21.0 ± 0.2 d | 1.18 ± 0.01 c | 0.19 ± 0.00 d | 7.5 ± 0.1 b | 27.0 ± 0.2 c | 3.0 |
| ABA | 0 | Col-0 | 3.3 ± 0.1 a | 7.3 ± 0.2 a | 0.45 ± 0.02 a | 21.6 ± 0.2 a | 19.9 ± 0.2 a | 1.09 ± 0.01 a | 0.17 ± 0.01 a | 7.1 ± 0.1 a | 23.5 ± 0.2 a | NA |
| | | *cesa3$^{je5}$* | 4.2 ± 0.1 c | 7.9 ± 0.2 a | 0.57 ± 0.02 b | 22.5 ± 0.3 a | 20.9 ± 0.2 c | 1.08 ± 0.01 a | 0.20 ± 0.01 c | 7.6 ± 0.1 b | 25.0 ± 0.3 b | NA |
| | 2.5 | Col-0 | 0.6 ± 0.0 b | 8.9 ± 0.4 b | 0.06 ± 0.01 c | 23.9 ± 0.5 b | 17.0 ± 0.2 b | 1.40 ± 0.02 b | 0.03 ± 0.00 b | 7.0 ± 0.1 a | 23.1 ± 0.4 a | −0.4 |
| | | *cesa3$^{je5}$* | 1.5 ± 0.1 d | 7.9 ± 0.2 a | 0.20 ± 0.02 d | 22.4 ± 0.3 a | 18.4 ± 0.1 d | 1.22 ± 0.02 c | 0.09 ± 0.01 d | 7.5 ± 0.1 b | 23.3 ± 0.2 a | −1.7 |

significantly higher aperture-guard cell pair width ratio at the beginning or the end of the 2.5-h FC or ABA treatment (Table I), suggesting that increased guard cell pair width is not the only contributor to the larger stomatal apertures observed in *cesa3$^{je5}$* mutants.

To test whether the larger stomatal aperture phenotype results from less restriction on radial expansion or from more longitudinal expansion in *cesa3$^{je5}$* guard cells during stomatal responses, we measured the diameters and lengths of individual guard cells (for measurement legend in a stomatal complex, see Supplemental Fig. S6) at the beginning and the end of 2.5-h FC treatments in Col-0 controls and *cesa3$^{je5}$* mutants. Although average guard cell diameter was significantly larger in *cesa3$^{je5}$* mutants than in Col-0 controls, guard cell diameter did not change significantly in either genotype during FC-induced stomatal opening (Table I; Supplemental Fig. S9D). In Col-0 controls, there was a slight but not significant increase in average guard cell length after FC treatment for 2.5 h, whereas in *cesa3$^{je5}$* mutants, this increase was statistically significant and more prominent (Table I; Supplemental Fig. S9E). We also did not observe significant changes in guard cell diameter during ABA-induced stomatal closure in either genotype, although average guard cell diameter remained significantly larger in *cesa3$^{je5}$* mutants than in Col-0 controls (Table I; Supplemental Fig. S9F). Again, in Col-0 controls, there was a slight but not significant decrease in average guard cell length after ABA treatment for 2.5 h, while in *cesa3$^{je5}$* mutants, this reduction was statistically significant and more prominent (Table I; Supplemental Fig. S9G). These data rule out the hypothesis that the regulation of radial expansion in guard cells during stomatal responses is defective in the *cesa3$^{je5}$* mutant and, instead, indicate that longitudinal expansion and contraction of guard cells is more facile in *cesa3$^{je5}$* mutants compared with wild-type controls, giving rise to larger stomatal apertures.

To confirm that cellulose is required to control stomatal aperture, we next conducted exactly the same set of experiments and measurements in transgenic plants expressing GFP-CESA3 in the *cesa3$^{je5}$* mutant background (Desprez et al., 2007). When grown in soil, 3-week-old GFP-CESA3 transgenic plants still displayed smaller rosettes than wild-type controls, but the timing of leaf emergence was more similar to Col-0 plants than to *cesa3$^{je5}$* mutants (Supplemental Fig. S10, A–C). GFP-CESA3 expression partially rescued the reduction in cellulose content in *cesa3$^{je5}$* rosette leaves as measured by Updegraff analysis but fully complemented the decrease in S4B staining fluorescence intensity observed in *cesa3$^{je5}$* guard cells (Table II). GFP-CESA3 expression also largely restored stomatal responses to FC and ABA treatments to levels comparable to wild-type controls, except at 0 h during the ABA treatment (Fig. 4, C and D). When measuring the geometry of stomatal pores, GFP-CESA3 stomata had smaller pore lengths, resulting in slightly higher ratios of aperture to pore length (Table III). When measuring the dimensions of guard cell pairs, GFP-CESA3 expression led to smaller guard

**Table II.** *Quantifications of cellulose content in Col-0, cesa3$^{je5}$, and GFP-CESA3 plants*

Cellulose content was quantified by the Updegraff method using 23-d-old rosette leaves or by analyzing S4B fluorescence intensity in guard cells from 3- to 4-week-old plants. Values are presented as means ± SE, and lowercase letters represent significantly different groups ($n \geq 10$ technical replicates from two biological replicates per genotype for the Updegraff method and $n \geq 60$ guard cells from three experiments per genotype for quantification of S4B fluorescence intensity; $P < 0.05$, one-way ANOVA and Tukey's test). AFU, Arbitrary fluorescence units.

| Genotype | Cellulose Content by the Updegraff Method | S4B Fluorescence Intensity in Guard Cells |
|---|---|---|
| | $\mu g\ mg^{-1}$ | $AFU\ \mu m^{-2}$ |
| Col-0 | 114.1 ± 4.7 a | 574,977 ± 39,350 a |
| *cesa3$^{je5}$* | 63.0 ± 3.1 b | 318,930 ± 33,171 b |
| GFP-CESA3 | 81.4 ± 2.2 c | 570,801 ± 43,095 a |

cell pair height but larger guard cell pair width, lower aspect ratio, and largely the same aperture-guard cell pair ratio compared with wild-type controls during FC or ABA treatment (Table III). When measuring the diameters and lengths of individual guard cells, there was no significant difference in guard cell diameter between genotypes or between different time points during FC or ABA treatment (Table III; Supplemental Fig. S10, D and F). The increase in average guard cell length during FC treatment or the decrease in average guard cell length during ABA treatment was similar between Col-0 controls and GFP-CESA3 transgenic plants, although guard cell length on average was consistently smaller in GFP-CESA3 plants than in Col-0 controls (Table III; Supplemental Fig. S10, E and G). Together, these results suggest that sufficient cellulose biosynthesis is required to regulate the longitudinal expansion of guard cells and, thus, for the proper control of stomatal aperture.

To further examine whether cellulose deficiency causes larger stomatal apertures, we treated epidermal peels from approximately 3-week-old Col-0 plants with cellulose-specific endo-1,4-β-D-glucanase (CEG) and induced stomatal opening by FC. Compared with the control condition, incubation with CEG did not lead to any significant change in stomatal aperture at the beginning of the 2.5-h FC treatment but resulted in a significant increase in stomatal aperture after FC treatment for 2.5 h (Supplemental Fig. S11, A and B). As an alternative approach, we applied a cellulose biosynthesis inhibitor, 2,6-dichlorobenzonitrile (DCB; DeBolt et al., 2007), to 6-d-old Col-0 seedlings and tested its effect on stomatal response to FC-induced opening. Stomata exposed to DCB for 2.5 h exhibited similar apertures to control stomata at the beginning of FC treatment but had significantly larger apertures at the end of FC treatment (Supplemental Fig. S11, C and D). To confirm the inhibition effect of DCB on cellulose biosynthesis, which is due to the hyper-accumulation and immobilization of CSCs at the plasma membrane (DeBolt et al., 2007), we found that CSC movement tracks disappeared in DCB-treated guard cells expressing GFP-CESA3 (Supplemental Fig. S11E). Taken together, these data suggest that cellulose deficiency by the degradation of existing cellulose or the inhibition of new cellulose biosynthesis can cause an increase in stomatal aperture in response to FC.

### Stomatal Apertures Are Smaller in the Xyloglucan-Deficient *xxt1 xxt2* Mutants

To investigate whether xyloglucan, the most abundant hemicellulose in eudicot primary walls (Zablackis et al., 1995), is required for stomatal development and/or function, we first performed PI staining of 6-d-old cotyledons in Col-0 and *xxt1 xxt2* seedlings, the latter of which lack two *XYLOGLUCAN XYLOSYLTRANSFERASE* genes and do not contain detectable xyloglucan (Cavalier et al., 2008; Park and Cosgrove, 2012a). *xxt1 xxt2* mutants exhibited wild-type stomatal patterning, with low percentages of paired stomata that deviated from the one-cell-spacing rule (6.6% ± 0.4% for *xxt1 xxt2* versus 4.8% ± 0.5% for Col-0; $n > 450$ stomata from 18 seedlings per genotype, three independent experiments; $P = 0.4$, $\chi^2$ test; Supplemental Fig. S12A). *xxt1 xxt2* mutants had smaller rosettes as well as smaller rosette leaves when grown in soil (Supplemental Fig. S12, B and C), as has been reported elsewhere (Cavalier et al., 2008; Park and Cosgrove, 2012a; Xiao et al., 2016). We found that, in contrast to *cesa3$^{je5}$* mutants, *xxt1 xxt2* plants have rosette leaf emergence patterns that are indistinguishable from wild-type controls (Supplemental Fig. S12, B and C). We next measured stomatal apertures every 0.5 h during FC-induced opening and ABA-induced closure in Col-0 and *xxt1 xxt2* plants over the course of 2.5 h. During the 2.5-h FC treatment, *xxt1 xxt2* apertures were significantly smaller than Col-0 apertures at all time points (Fig. 5A). Likewise, during ABA-induced stomatal closure, the average apertures of *xxt1 xxt2* stomata were smaller than Col-0 controls at all time points except 1.5 h (Fig. 5B). Over the total 2.5-h treatments, FC induced a larger percentage increase in average aperture in *xxt1 xxt2* stomata (299.3%) than in Col-0 controls (256.7%), and ABA induced a slightly larger percentage decrease in average aperture in *xxt1 xxt2* stomata (76.8%) than in Col-0 controls (73.3%).

We next asked whether the reduced aperture of *xxt1 xxt2* stomata is due to smaller overall pore size. We measured pore length and the ratio of aperture to pore length on a single stomate basis in Col-0 controls and the double mutant. In general, *xxt1 xxt2* stomata had smaller pore lengths and lower aperture-to-pore length

**Table III.** *Stomatal pore dimensions, guard cell pair dimensions, and guard cell dimensions in wild-type and GFP-CESA3 plants during FC or ABA treatment*

Stomatal aperture, stomatal pore length, ratio of aperture to pore length, guard cell pair height, guard cell pair width, aspect ratio of guard cell pairs (height to width), ratio of aperture to guard cell pair width, guard cell diameter, and guard cell length were measured on a single stomate basis using epidermal peels from 3- to 4-week-old plants. Values are presented as means ± SE ($n > 90$ stomata for each genotype at each time point from three experiments). Lowercase letters represent significantly different groups ($P < 0.05$, one-way ANOVA and Tukey's test). ANOVA was performed within each treatment. NA, Not applicable.

| Treatment | Time after Treatment | Genotype | Average Stomatal Aperture | Average Stomatal Pore Length (μm) | Average Ratio of Aperture to Pore Length | Average Guard Cell Pair Height | Average Guard Cell Pair Width (μm) | Average Aspect Ratio of Guard Cell Pairs | Average Ratio of Aperture to Guard Cell Pair Width | Average Guard Cell Diameter | Average Guard Cell Length (μm) | Change in Average Guard Cell Length (μm) |
|---|---|---|---|---|---|---|---|---|---|---|---|---|
| | *h* | | *μm* | | | *μm* | | | | *μm* | | |
| FC | 0 | Col-0 | 0.7 ± 0.0 a | 11.6 ± 0.2 a | 0.05 ± 0.00 a | 26.1 ± 0.2 a | 17.0 ± 0.2 a | 1.55 ± 0.02 a | 0.03 ± 0.00 a | 7.5 ± 0.1 a | 25.0 ± 0.2 a | NA |
| | | GFP-CESA3 | 0.7 ± 0.0 a | 8.7 ± 0.2 b,c | 0.07 ± 0.01 a | 23.9 ± 0.3 b | 17.7 ± 0.1 c | 1.36 ± 0.02 c | 0.03 ± 0.00 a | 7.4 ± 0.0 a | 23.3 ± 0.2 b | NA |
| | 2.5 | Col-0 | 2.4 ± 0.1 b | 9.3 ± 0.2 b | 0.30 ± 0.01 b | 23.9 ± 0.3 b | 19.0 ± 0.2 b | 1.26 ± 0.01 b | 0.14 ± 0.00 b | 7.3 ± 0.1 a | 25.7 ± 0.3 a | 0.7 |
| | | GFP-CESA3 | 2.5 ± 0.1 b | 8.0 ± 0.2 c | 0.36 ± 0.01 c | 22.6 ± 0.2 c | 19.5 ± 0.2 b | 1.17 ± 0.01 d | 0.14 ± 0.00 b | 7.3 ± 0.1 a | 23.8 ± 0.2 b | 0.5 |
| ABA | 0 | Col-0 | 2.8 ± 0.1 a | 9.4 ± 0.2 a | 0.30 ± 0.01 a | 23.2 ± 0.2 a | 19.8 ± 0.1 a | 1.18 ± 0.01 a | 0.16 ± 0.00 a | 7.5 ± 0.1 a | 24.9 ± 0.2 a | NA |
| | | GFP-CESA3 | 3.5 ± 0.1 c | 7.5 ± 0.1 b | 0.52 ± 0.02 b | 20.9 ± 0.2 c | 20.3 ± 0.1 c | 1.03 ± 0.01 c | 0.19 ± 0.00 c | 7.5 ± 0.0 a | 23.6 ± 0.1 b | NA |
| | 2.5 | Col-0 | 0.6 ± 0.0 b | 9.0 ± 0.2 a | 0.05 ± 0.00 c | 24.4 ± 0.3 b | 17.0 ± 0.1 b | 1.44 ± 0.02 b | 0.03 ± 0.00 b | 7.5 ± 0.0 a | 24.0 ± 0.2 b | −0.9 |
| | | GFP-CESA3 | 0.6 ± 0.0 b | 8.0 ± 0.1 c | 0.06 ± 0.00 c | 23.0 ± 0.2 a | 17.4 ± 0.1 b | 1.33 ± 0.01 d | 0.03 ± 0.00 b | 7.5 ± 0.0 a | 22.9 ± 0.2 c | −0.7 |

ratios than wild-type stomata (Table IV). We also measured the heights and widths of guard cell pairs at the beginning and end of the 2.5-h FC or ABA treatment. *xxt1 xxt2* guard cell pairs exhibited slight reductions in both dimensions in comparison with Col-0 controls (Table IV). The diminished stomatal apertures in the *xxt1 xxt2* mutants could be attributed to the relatively smaller guard cell pair size in the double mutants (Table IV). To test this possibility, we measured aperture-guard cell pair width ratios in both Col-0 and *xxt1 xxt2* guard cell pairs and found that the double mutants had significantly smaller ratios than wild-type controls during ABA treatment (Table IV), suggesting that the slightly reduced size of guard cell pairs is less likely to account for the smaller stomatal apertures in the *xxt1 xxt2* mutants.

To test how the smaller stomatal apertures in *xxt1 xxt2* mutants relate to guard cell geometry, we measured the diameters and lengths of individual guard cells. There was no significant difference in average guard cell diameter between Col-0 controls and *xxt1 xxt2* mutants or between 0 or 2.5 h during the 2.5-h course of FC or ABA treatment (Table IV; Supplemental Fig. S12, D and F). However, the increase in average guard cell length after FC treatment for 2.5 h and the decrease in average guard cell length after ABA treatment for 2.5 h were lower in *xxt1 xxt2* mutants than in wild-type controls (Table IV; Supplemental Fig. S12, E and G). These results suggest that *xxt1 xxt2* guard cells have comparable constraints on radial expansion but exhibit reduced longitudinal expansion and contraction compared with Col-0 controls. Together, these data indicate that xyloglucan in guard cell walls facilitates their longitudinal expansion, thus regulating stomatal aperture.

### Cellulose in Guard Cell Walls Undergoes Significant Reorganization during Stomatal Movement in Col-0 and GFP-CESA3 Plants But Not in *cesa3$^{je5}$*, *xxt1 xxt2*, or *cesa7$^{irx3\text{-}5}$* Mutants

The radial arrangement of cellulose in guard cell walls has long been hypothesized to constrain guard cell expansion during stomatal responses (Wu et al., 1985). We next tested whether cellulose undergoes rearrangements during stomatal opening and closing and explored the mechanism(s) by which alterations in cellulose organization might be connected to the stomatal phenotypes we observed in mutants with defects in cellulose or xyloglucan biosynthesis, using S4B staining in guard cells. We found that, in the Col-0 ecotype, S4B staining revealed a more diffuse distribution of cellulose in guard cells bordering open stomata induced by FC or light (Fig. 6, A and B) while a subtly more fibrillar pattern was evident in guard cells surrounding closed stomata induced by ABA or dark treatment (Fig. 6, C and D). Anisotropy assessment of S4B-stained cellulose organization using the FibrilTool plugin for ImageJ (Boudaoud et al., 2014) showed that guard cells in the closed state had significantly higher

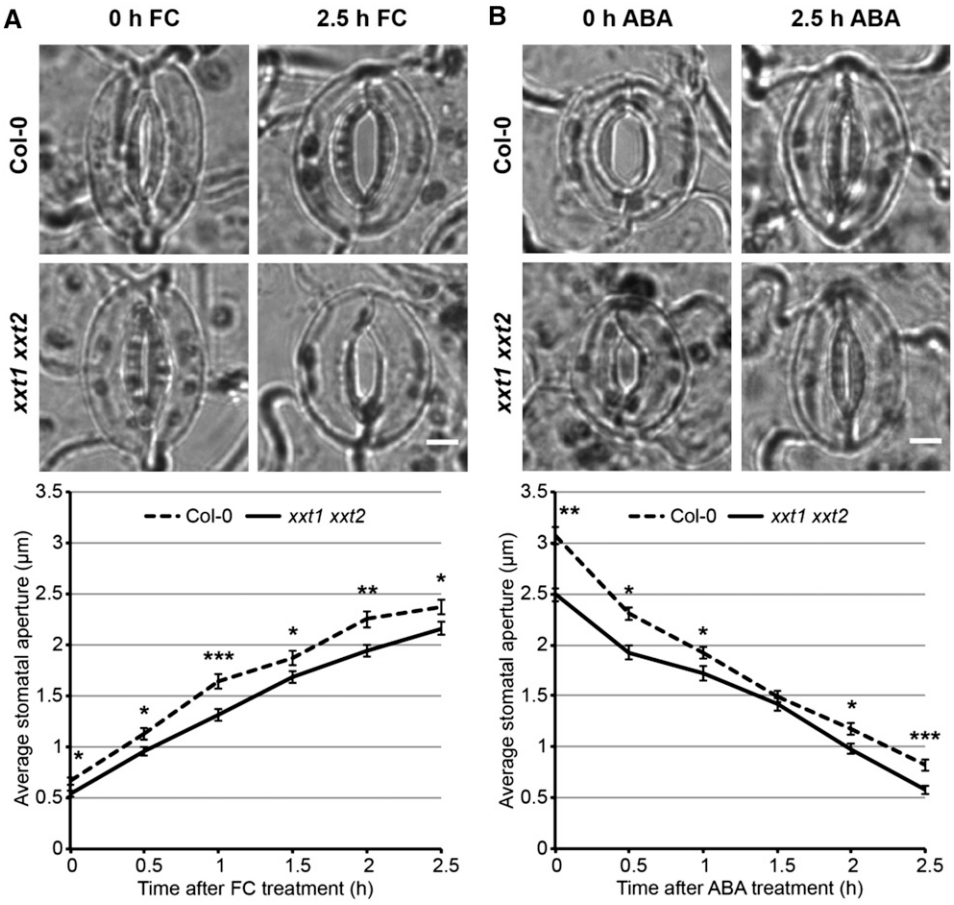


**Figure 5.** Stomatal responses to FC or ABA in *xxt1 xxt2* mutants. A, Time-course stomatal responses to 1 $\mu$M FC-induced opening in Col-0 and *xxt1 xxt2* epidermal peels, with representative bright-field stomatal images at the top and measurements of stomatal apertures at the bottom. Error bars indicate SE. Asterisks indicate significant differences between genotypes at each time point examined ($n$ = approximately 120 stomata per genotype per time point from three independent experiments; *, $P < 0.05$, **, $P < 0.01$, and ***, $P < 0.001$, Student's $t$ test). Bar = 5 $\mu$m. B, Time-course stomatal responses to 50 $\mu$M ABA-induced closure in Col-0 and *xxt1 xxt2* epidermal peels, with representative bright-field stomatal images at the top and measurements of stomatal apertures at the bottom. Error bars indicate SE. Asterisks indicate significant differences between genotypes at each time point examined ($n > 80$ stomata per genotype per time point from two independent experiments; *, $P < 0.05$, **, $P < 0.01$, and ***, $P < 0.001$, Student's $t$ test). Bar = 5 $\mu$m.

anisotropy scores than those in the open state (Fig. 6E). We next performed identical experiments in *cesa3*$^{je5}$, *cesa3*$^{eli1\text{-}1}$, *cesa6*$^{prc1\text{-}1}$, GFP-CESA3, and *xxt1 xxt2* plants. Cellulose distribution patterns as well as anisotropy degrees in the *cesa3*$^{eli1\text{-}1}$ and *cesa6*$^{prc1\text{-}1}$ mutants were indistinguishable from wild-type controls in the open or closed state induced by light or dark treatment (Supplemental Fig. S13). In contrast to Col-0 controls, cellulose organization in open and closed *cesa3*$^{je5}$ guard cells appeared to be very similar (Fig. 6, F–I), with degrees of anisotropy that were slightly lower than in Col-0 controls in the open state, were significantly lower than in Col-0 controls in the closed state, and did not differ significantly between open and closed states (Fig. 6, E, J, and U). GFP-CESA3 expression in the *cesa3*$^{je5}$ mutant background restored the distinct cellulose distribution patterns between open and closed states, with anisotropy scores being significantly higher in the closed state than in the open state (Fig. 6, K–O) and higher than the corresponding Col-0 values in each treatment (Fig. 6U). In the case of *xxt1 xxt2* guard cells, S4B-stained fibrillar patterns were evident in both open and closed stomata (Fig. 6, P–S), with no significant change between the two states in anisotropy values (Fig. 6T), which were intermediate between those of Col-0 open and closed stomatal guard cells (Fig. 6, E, T, and U). Overall, these results indicate that cellulose in wild-type Arabidopsis guard cell walls undergoes reorganization from a relatively even distribution in the open state to extensive bundling in the closed state and that sufficient amounts of cellulose and xyloglucan allow for such reorganization.

We also characterized the organization of cellulose in open versus closed guard cells of a secondary wall-associated CESA mutant, *cesa7*$^{irx3\text{-}5}$, which was reported to have smaller guard cells and smaller stomatal apertures due to collapsed vasculature and compromised water transport (Liang et al., 2010). Compared with Columbia-2 (Col-2) control guard cells, which exhibited reorganization of cellulose and a significant change in anisotropy score between open and closed states (Supplemental Fig. S14, A–E), *cesa7*$^{irx3\text{-}5}$ guard cells in both open and closed states had fibrillar S4B staining patterns that were comparable to those of closed Col-2 guard cells (Supplemental Fig. S14, F–J). We also measured S4B fluorescence intensity in Col-2 and *cesa7*$^{irx3\text{-}5}$ guard cells using the same image set and found no significant difference between the two genotypes (499,160 $\pm$ 25,310 for Col-2 versus 482,786 $\pm$ 30,412 for *cesa7*$^{irx3\text{-}5}$; $n \geq 87$ guard cells per genotype, three independent experiments; $P = 0.68$, Student's $t$ test). These data suggest that the lack of cellulose reorganization

**Table IV.** *Stomatal pore dimensions, guard cell pair dimensions in wild-type and xxt1 xxt2 plants during FC or ABA treatment*

Stomatal aperture, stomatal pore length, ratio of aperture to pore length, guard cell pair height, guard cell pair width, aspect ratio of guard cell pairs (height to width), ratio of aperture to guard cell pair width, guard cell diameter, and guard cell length were measured on a single stomate basis using epidermal peels from 3- to 4-week-old plants. Values are presented as means ± SE ($n >$ 80 stomata for each genotype at each time point from three experiments). Lowercase letters represent significantly different groups ($P < 0.05$, one-way ANOVA and Tukey's test). ANOVA was performed within each treatment. NA, Not applicable.

| Treatment | Time after Treatment | Genotype | Average Stomatal Aperture | Average Stomatal Pore Length (μm) | Average Ratio of Aperture to Pore Length | Average Guard Cell Pair Height | Average Guard Cell Pair Width (μm) | Average Aspect Ratio of Guard Cell Pairs | Average Ratio of Aperture to Guard Cell Pair Width | Average Guard Cell Diameter | Average Guard Cell Length (μm) | Change in Average Guard Cell Length (μm) |
|---|---|---|---|---|---|---|---|---|---|---|---|---|
| | *h* | | *μm* | | | *μm* | | | | *μm* | | |
| FC | 0 | Col-0 | 0.7 ± 0.0 a | 10.9 ± 0.2 a | 0.06 ± 0.00 a | 26.5 ± 0.2 a | 18.1 ± 0.1 a | 1.47 ± 0.01 a | 0.03 ± 0.00 a | 7.6 ± 0.1 a | 25.4 ± 0.2 a | NA |
| | | *xxt1 xxt2* | 0.5 ± 0.0 a | 9.7 ± 0.2 b | 0.05 ± 0.00 a | 25.2 ± 0.2 b | 18.0 ± 0.1 a | 1.40 ± 0.01 c | 0.03 ± 0.00 a | 7.5 ± 0.1 a | 24.7 ± 0.2 a | NA |
| | 2.5 | Col-0 | 2.4 ± 0.1 b | 12.2 ± 0.3 c | 0.23 ± 0.01 b | 26.8 ± 0.3 a | 20.4 ± 0.2 b | 1.32 ± 0.01 b | 0.12 ± 0.00 b | 7.5 ± 0.1 a | 26.7 ± 0.3 b | 1.3 |
| | | *xxt1 xxt2* | 2.2 ± 0.1 b | 9.9 ± 0.2 b | 0.25 ± 0.01 c | 24.1 ± 0.2 c | 19.9 ± 0.1 b | 1.21 ± 0.01 d | 0.12 ± 0.00 b | 7.6 ± 0.1 a | 25.0 ± 0.2 a | 0.3 |
| ABA | 0 | Col-0 | 3.1 ± 0.1 a | 10.8 ± 0.2 a | 0.25 ± 0.01 a | 24.6 ± 0.3 a | 20.0 ± 0.2 a | 1.24 ± 0.01 a | 0.14 ± 0.00 a | 7.5 ± 0.1 a | 25.1 ± 0.2 a | NA |
| | | *xxt1 xxt2* | 2.5 ± 0.1 c | 10.1 ± 0.2 b | 0.20 ± 0.01 b | 24.0 ± 0.3 a | 19.1 ± 0.2 c | 1.25 ± 0.01 a | 0.12 ± 0.00 c | 7.4 ± 0.1 a | 25.1 ± 0.3 a | NA |
| | 2.5 | Col-0 | 0.8 ± 0.1 b | 10.2 ± 0.2 a,b | 0.06 ± 0.00 c | 24.9 ± 0.3 a | 17.5 ± 0.2 b | 1.43 ± 0.02 b | 0.03 ± 0.00 b | 7.5 ± 0.1 a | 24.4 ± 0.2 a | −0.7 |
| | | *xxt1 xxt2* | 0.6 ± 0.0 d | 10.3 ± 0.2 a,b | 0.05 ± 0.00 c | 24.6 ± 0.3 a | 17.1 ± 0.2 b | 1.45 ± 0.02 b | 0.02 ± 0.00 d | 7.4 ± 0.1 a | 24.8 ± 0.2 a | −0.3 |

observed in *cesa7*$^{irx3\text{-}5}$ guard cells is not due to cellulose deficiency but might be an indirect effect of defective water transpiration on stomatal development.

## DISCUSSION

In this work, we used live-cell spinning disk confocal microscopy to image CSC distribution and motility in stomatal guard cells in young tissues and observed several intriguing patterns of CSC activity. FP-labeled CESA1, CESA3, and CESA6 particles show significant reductions in density in guard cells as plants mature (Supplemental Fig. S1), a finding that contrasts with previous guard cell-specific transcriptome data, in which primary wall *CESA*s were detected as being highly expressed in guard cells or guard cell protoplasts prepared from mature rosette leaves (Yang et al., 2008; Bates et al., 2012). A possible explanation for this inconsistency between *CESA* gene expression levels and our FP-CESA density data is that transcript abundance, protein abundance, protein stability, and protein localization are not always correlated with each other. Alternatively, the transcriptome data might be confounded by changes in gene expression in response to stresses during sample preparation procedures, which involve cellulase treatment or freeze-drying (Yang et al., 2008; Bates et al., 2012). Another possibility is that CSCs containing the secondary wall-associated CESA isoform, CESA4, CESA7, or CESA8, generate additional cellulose to enable stomatal functions in mature plants, although *CESA4*, *CESA7*, or *CESA8* has not been reported to be highly expressed in guard cells (Yang et al., 2008; Bates et al., 2012).

The speed of FP-labeled CESA movement can be used as a proxy for the rate of nascent cellulose biosynthesis and potentially can be affected by the availability of UDP-Glc as the substrate, posttranslational regulation of CESAs in response to environmental cues, and/or interactions between CSCs and MTs (McFarlane et al., 2014). The observations that GFP-CESA3 particle movement is faster in guard cells bordering closed stomata as well as in neighboring pavement cells in 6-d-old seedlings after ABA or 2.5-h dark treatment (Fig. 1; Supplemental Fig. S3 and S4) are counterintuitive, especially in the latter case, as one would expect a reduced photosynthetic production of Glc, which is a precursor of UDP-Glc. A recent study in Arabidopsis rosette leaves suggested that photosynthesis impacts cellulose biosynthesis via an increase of carbon flux to cellulose and changes in CESA protein phosphorylation levels (Boex-Fontvieille et al., 2014), but the degree to which UDP-Glc production is altered during photosynthesis and the extent to which cellulose synthesis in guard cells depends on light remain unclear. In another study in *cesa6*$^{prc1\text{-}1}$ mutants, dark-grown hypocotyls had lower CSC motility than light-grown hypocotyls, but a short-term treatment of dark-grown hypocotyls with red light increased CSC motility to levels comparable to light-grown hypocotyls. This effect of red light requires the presence of the red photoreceptor phytochrome B,

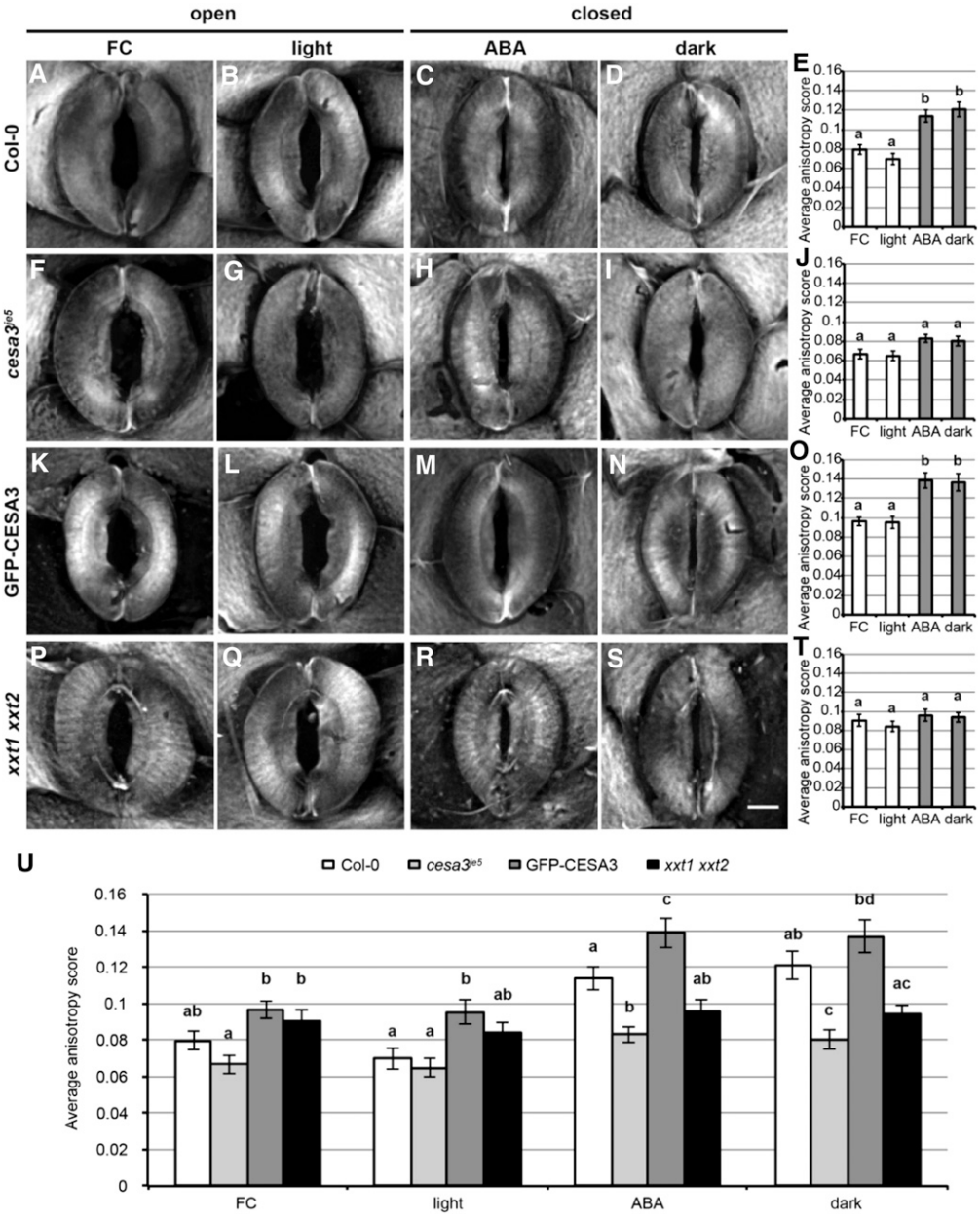


**Figure 6.** S4B labeling of cellulose in Col-0, *cesa3*$^{je5}$, GFP-CESA3, and *xxt1 xxt2* guard cells with open or closed stomata. A to D, F to I, K to N, and P to S, Maximum projections of S4B staining pattern in guard cells from rosette leaves. Stomatal opening was induced by 1 $\mu$M FC for 2.5 h (A, F, K, and P) or light for 2.5 h (B, G, L, and Q). Stomatal closure was induced by 50 $\mu$M ABA for 2.5 h (C, H, M, and R) or dark treatment for 2.5 h (D, I, N, and S). Bar in S = 5 $\mu$m. E, J, O, T, and U, Anisotropy quantification of S4B-stained cellulose in guard cells within each genotype (E, J, O, and T) and within each treatment across genotypes (U). Error bars indicate SE, and lowercase letters represent significantly different groups ($n \geq 12$ guard cell pairs per genotype per treatment; $P < 0.05$, one-way ANOVA and Tukey's test). ANOVA was performed within each genotype in E, J, O, and T and within each treatment in U.

suggesting that cellulose biosynthesis might be a downstream target of phytochrome B-involved light signaling pathways in *cesa6*$^{prc1\text{-}1}$ hypocotyls (Bischoff et al., 2011). The discrepancy in the effect of darkness on CSC motility between our results in guard cells and the previous results in *cesa6*$^{prc1\text{-}1}$ hypocotyls (Bischoff et al., 2011) could be attributed to the tissue specificity of dark-responsive signaling or different durations of dark treatment. We speculate that the increase in GFP-CESA3 speed in guard cells bordering closed stomata and in neighboring pavement cells, in light of the findings from previous studies (Bischoff et al., 2011; Boex-Fontvieille et al., 2014), might be attributed, at least in part, to posttranslational modulation of CESA3

as a downstream effect of darkness or ABA signaling. The GFP-CESA3 motility results, taken together with FP-CESA density data in guard cells from plants at different ages, lead us to hypothesize that cellulose is deposited in guard cells during early plant development, more so when stomata are closed. When plants become mature with sufficient wall thickness, guard cells might discontinue cellulose biosynthesis and use existing cellulose to fulfill stomatal function for their remaining lifetimes.

CSCs migrate at the plasma membrane in linear trajectories coaligned with underlying cortical MTs, the presence of which is not a strict requirement for CSC motility (Paredez et al., 2006; Chen et al., 2010). Although CELLULOSE SYNTHASE INTERACTIVE1 (CSI1), and to a lesser degree CSI3, have been identified as linking CSCs and MTs (Gu et al., 2010; Li et al., 2012; Lei et al., 2013), the mechanisms for MT-independent CSC movement are poorly understood. Dual-channel imaging of GFP-CESA3 and mCherry-TUA5 allowed us to analyze the colocalization of CSCs and MTs in stomatal guard cells (Fig. 2). The degree of colocalization in guard cells was not as high as that reported previously in dark-grown hypocotyls (Paredez et al., 2006; Li et al., 2012), suggesting that the behavior of CSCs is cell type specific. Previous research in guard cells expressing GFP-tagged tubulin revealed a decrease in cortical MTs upon stomatal closure (Eisinger et al., 2012a, 2012b). However, our quantifications of mCherry-TUA5-labeled MT fluorescence area and intensity in guard cells did not show any significant differences between open and closed stomata (Supplemental Table S1), ruling out the possibility that the reduced degree of CSC-MT colocalization we observed upon stomatal closure is due to fewer MTs for CSCs to move along. Other explanations are that, as stomata close, there is a disruption in the guidance of CSCs by MTs or a time lag between changes in MT dynamics and CSC translocation. Alternatively, the decreased proportion of CSCs colocalizing with MTs could be attributed to the dynamic turnover of CESA particles at the plasma membrane, given that the lifetime of a typical CESA particle in the plasma membrane is approximately 7 min (Sampathkumar et al., 2013). In other words, the GFP-CESA3 particles in partially closed guard cells after dark treatment for 30 min might be newly delivered to the plasma membrane and consist of a different set of GFP-CESA3 particles than those in open guard cells under light control conditions. Combining the colocalization results with the aforementioned CSC activity data, it is possible that CSCs in guard cells bordering closed stomata in young tissues might move faster when traveling independently of MTs, an idea that is also suggested by two other previous reports in Arabidopsis dark-grown hypocotyls (Bischoff et al., 2011; Fujita et al., 2011), in which MT depolymerization by oryzalin (Bischoff et al., 2011) or MT disruption by mutation of *MICROTUBULE ORGANIZATION1* (Fujita et al., 2011) resulted in increased CSC motility. In addition, we did not detect a significant change in the colocalization of GFP-CESA3 particles and MTs in pavement cells adjacent to guard cells (Supplemental Fig. S5), indicating that a reduction in colocalization in response to dark treatment for 30 min is unique to guard cells in the epidermis. Therefore, we argue that the aforementioned CESA3 posttranslational modification(s) might be a common mechanism underlying the faster movement of GFP-CESA3 particles in both guard cells bordering closed stomata and neighboring pavement cells in young tissues, but this mechanism might be independent of the reduced interaction between CSCs and MTs, which was observed only in guard cells.

Our Updegraff measurement of approximately 11% cellulose content in Col-0 rosette leaves (Fig. 3; Table II) is slightly lower but comparable to a previously published result, which is around 14% of leaf cell walls (Zablackis et al., 1995). To estimate cellulose content specifically in guard cells, we used fluorescence intensity from S4B staining or CBM3a immmunolabeling of cellulose. These two methods did not yield identical spatial patterns of labeling in guard cells (Fig. 6; Supplemental Fig. S7), which could be due to differences in diffusability, given that S4B is a small molecule (Anderson et al., 2010), whereas CBM3a is a large proteinaceous molecule (Tormo et al., 1996)*cesa3*$^{je5}$ guard cells consistently had the most severe reduction in fluorescence intensity among all *cesa* mutants examined (Fig. 3). More broadly, we found a correlation between the degree of decrease in cellulose content in guard cells and aberrant stomatal apertures during light treatment in *cesa3*$^{je5}$, *cesa3*$^{eli1\text{-}1}$, and *cesa6*$^{prc1\text{-}1}$ mutants (Fig. 3), indicating that a sufficient amount of cellulose in guard cells is required for the control of normal stomatal aperture. It is also intriguing that, despite low cellulose content in the *cesa3*$^{je5}$ mutants (around 6% of leaf cell wall by the Updegraff method; Fig. 3; Table II), rosette leaves still develop and grow, although in a delayed and dwarfed manner (Supplemental Fig. S9). It is possible that the amounts of matrix wall polymers or the interactions between existing cellulose and other wall components are altered to compensate for cellulose deficiency in *cesa3*$^{je5}$ mutants.

Our finding that *cesa3*$^{je5}$ mutant seedlings have an approximately 3-fold increase in paired stomata over wild-type controls (Supplemental Fig. S8) supports the hypothesis that perturbation of cellulose production can lead to stomatal cluster formation, an idea proposed in a previous study of the glycosyltransferase-like protein KOBITO1, which is involved in cellulose biosynthesis (Kong et al., 2012). However, exactly how cellulose biosynthesis is involved in regulating stomatal patterning requires further investigation. When examining stomatal responses to FC or ABA treatment, we found that *cesa3*$^{je5}$ mutants exhibited larger stomatal apertures than wild-type controls (Fig. 4). Reasoning that an overall larger stomatal pore dimension or a larger guard cell pair size could contribute to a larger aperture, we measured various parameters to test this possibility. The result that stomatal aperture-to-pore

length ratios are consistently larger in *cesa3*$^{je5}$ mutants than in wild-type controls (Table I) rules out the hypothesis that larger apertures in *cesa3*$^{je5}$ stomata are simply due to altered stomatal size. Although we found that *cesa3*$^{je5}$ mutants had larger guard cell pair widths (Table I), this phenotype is not likely to account for the larger stomatal apertures of *cesa3*$^{je5}$, as the ratio of stomatal aperture to guard cell pair width remained higher in *cesa3*$^{je5}$ compared with wild-type controls (Table I).

Cellulose microfibrils are necessary for anisotropic expansion in several types of elongating cells (Baskin, 2005), and because guard cell expansion during stomatal movement is minimized in the radial direction, one might expect that sufficient numbers of radially arranged cellulose microfibrils are required to restrict radial expansion during stomatal opening. However, our finding that there was no significant change in guard cell diameter after FC or ABA treatment in *cesa3*$^{je5}$ mutants (Table I; Supplemental Fig. S9) runs counter to this idea. Instead, the changes in guard cell length after FC or ABA treatment were greater in *cesa3*$^{je5}$ mutants than in Col-0 controls (Table I; Supplemental Fig. S9), suggesting that the longitudinal expansion and contraction of guard cells occurs more readily when there is insufficient cellulose and that a cellulose-independent mechanism might constrain radial expansion during stomatal dynamics. These observations in *cesa3*$^{je5}$ guard cells are inconsistent with the reduced growth phenotypes caused by more isotropic expansion in roots and hypocotyls of other primary wall CESA mutants such as *cesa1*$^{rsw1\text{-}1}$, *cesa3*$^{eli1\text{-}1}$, and *cesa6*$^{prc1\text{-}1}$ (Desnos et al., 1996; Arioli et al., 1998; Caño-Delgado et al., 2003), indicating that guard cells might respond to cellulose deficiency differently from root or hypocotyl cells, where growth arrest is a response to cell wall integrity sensing (Hématy et al., 2007; Wolf et al., 2012). Taken together, our data imply that cellulose deficiency results in more longitudinal expansibility of *cesa3*$^{je5}$ guard cells and, thus, larger apertures during stomatal movements.

In contrast to *cesa3*$^{je5}$, a secondary wall-associated CESA mutant, *cesa7*$^{irx3\text{-}5}$, exhibits smaller stomatal apertures due to smaller guard cells (Liang et al., 2010). The discrepancy in alterations in stomatal aperture between *cesa3*$^{je5}$ and *cesa7*$^{irx3\text{-}5}$ mutants is intriguing. We did not detect any significant difference in S4B staining fluorescence intensity in guard cells between wild-type controls and *cesa7*$^{irx3\text{-}5}$ mutants, indicating that *cesa7*$^{irx3\text{-}5}$ guard cells are unlikely to be deficient in cellulose and that cellulose in general is deposited during primary wall biosynthesis in guard cells. In addition, we did not observe phenotypes indicative of compromised water transport, such as wilted leaves, in the *cesa3*$^{je5}$ mutants. Therefore, we propose that cellulose deficiency in *cesa3*$^{je5}$ mutants more directly causes an increase in stomatal aperture, whereas in *cesa7*$^{irx3\text{-}5}$ mutants, the smaller stomatal aperture brought about by decreased guard cell size might be due to collapsed xylem and compromised water transport (Liang et al., 2010), as fluctuations of supply and demand during water movement across the plant can modulate stomatal development (Lake and Woodward, 2008).

GFP-CESA3 expression in the *cesa3*$^{je5}$ mutant background does not fully complement cellulose content in whole leaves (Table II) or rosette size to wild-type levels (Supplemental Fig. S10) but rescues the phenotypes of larger stomatal aperture (Fig. 4), larger guard cell diameter (Table III; Supplemental Fig. S10), and changes in guard cell length (Table III; Supplemental Fig. S10), confirming the function of cellulose in guard cell expansion and, thus, the control of stomatal aperture during stomatal movements. Cellulose content measured by the Updegraff method in the GFP-CESA3 transgenic rosette leaves is intermediate between those of *cesa3*$^{eli1\text{-}1}$ and *cesa6*$^{prc1\text{-}1}$ mutants (Fig. 3; Table II), but S4B staining fluorescence intensity in GFP-CESA3 guard cells is comparable to wild-type values (Table II), corroborating the aforementioned hypothesis that the maintenance of normal stomatal aperture requires a sufficient amount of cellulose in guard cells.

In addition to the above genetic evidence, the function of cellulose in controlling stomatal aperture is also supported by the results of our enzyme and drug treatment experiments (Supplemental Fig. S11). CEG hydrolyzes 1,4-$\beta$-glucan chains, and its application in wild-type epidermal peels results in larger stomatal aperture after FC treatment compared with control samples, which is consistent with the results for *ceas*$^{je5}$ mutants, which have larger stomatal apertures due to cellulose deficiency (Fig. 3). It is worth noting that non-cellulase-treated epidermal peels have relatively smaller average stomatal apertures (Supplemental Fig. S11) than the control samples used in other time-course FC treatments in this work (Tables I, II, and IV). One possible explanation for this difference is that epidermal peels were made before enzyme or control incubations for these experiments, whereas in the other time-course FC treatments, the epidermis was peeled off from intact leaves immediately before imaging. In a previous study, cellulase treatment of epidermal strips from *Commelina communis* led to normally opened stomata in response to FC, although other epidermal cell types were disrupted (Jones et al., 2003). We did not observe any detrimental effects on pavement cells in our cellulase treatment in Arabidopsis. This could be attributed to a difference in the type of cellulase used, the pH and temperature conditions of cellulase incubation, and/or plant species. DCB inhibits nascent cellulose biosynthesis by causing an overaccumulation of CSCs at the plasma membrane and halting their motility (DeBolt et al., 2007). Our observation that DCB-exposed stomata had an increase in stomatal aperture compared with control stomata provides additional evidence that cellulose deficiency causes larger stomatal apertures in response to FC.

Our analyses of stomatal apertures and guard cell dimensions in *xxt1 xxt2* stomata revealed new phenotypes in this double mutant (Fig. 5). The smaller stomatal apertures in response to FC and ABA and the result that guard cell diameter remained the same while

the change in guard cell length was slightly altered from the beginning to the end of FC or ABA treatment in the *xxt1 xxt2* mutants compared with wild-type controls (Table IV; Supplemental Fig. S12) indicate that guard cell walls lacking xyloglucan are less capable of longitudinal expansion during stomatal movement. This finding is in agreement with *xxt1 xxt2* walls in petioles being less extensible during $\alpha$-expansin-mediated wall-loosening processes as well as FC-induced growth, although the mutant petiole walls also showed higher mechanical compliance (Park and Cosgrove, 2012a). The slightly reduced guard cell pair size (Table IV) is compatible with the previous finding that *xxt1 xxt2* mutants are smaller overall than wild-type controls (Cavalier et al., 2008; Park and Cosgrove, 2012a). Mirroring *cesa3*$^{je5}$ mutants, the smaller stomatal apertures of *xxt1 xxt2* mutants are less likely to be attributable to a relatively smaller pore dimension or smaller guard cell pair size, as the ratio of stomatal aperture to pore length or the ratio of stomatal aperture to guard cell pair width is still lower in the double mutant compared with wild-type controls during the 2.5-h ABA treatment (Table IV).

Application of the cellulose-specific fluorescent dye S4B (Anderson et al., 2010) allowed us to examine the organization of cellulose in guard cells bordering open or closed stomata (Fig. 6; Supplemental Figs. S13 and S14). The implication of these results is that, during stomatal movement, cellulose in guard cells might reorganize from evenly distributed, closely spaced microfibrils in the open state to extensive bundles in the closed state. Such a reorganization differs from previous observations of cellulose reorientation in irreversibly expanding root cells (Anderson et al., 2010), since reorganization refers to organizational changes, such as changes in spacing, in the overall existing cellulose whereas reorientation involves directional movements of individual regions or fibers of cellulose. At this point, we cannot determine the cause-and-effect relationship between cellulose reorganization in guard cells and stomatal movement. However, we hypothesize that cellulose reorganization accommodates and might

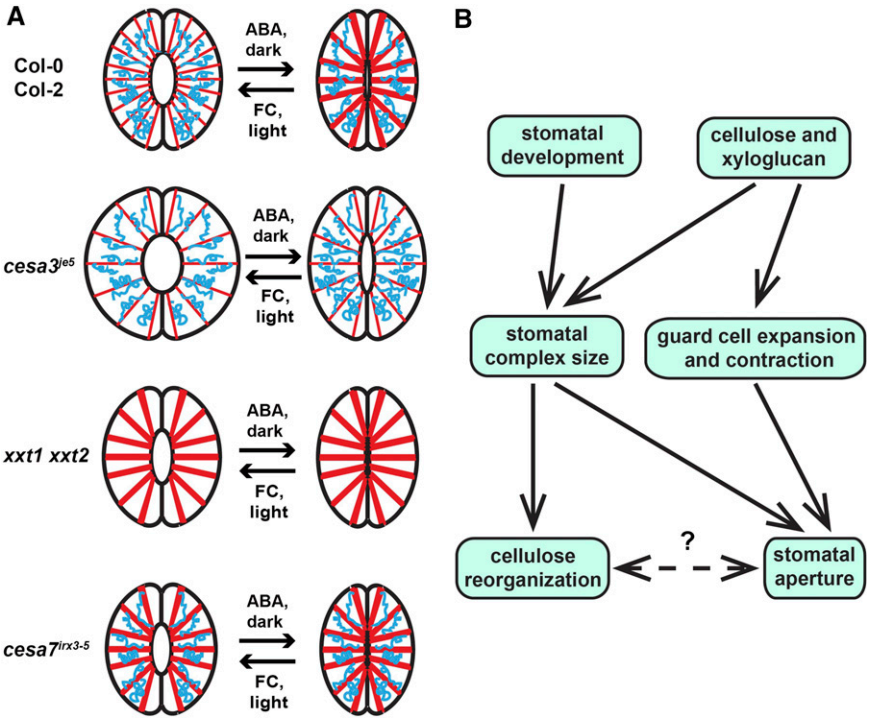


**Figure 7.** Models for cellulose and xyloglucan in guard cells during stomatal movement. A, Schematics summarizing stomatal aperture changes and cellulose organization patterns in wild-type, *cesa3*$^{je5}$, *xxt1 xxt2*, and *cesa7*$^{irx3-5}$ stomata. Cellulose is represented as red spokes, and xyloglucan is demonstrated as blue coils that interact with cellulose microfibrils at limited regions. With sufficient amounts of cellulose and xyloglucan present in guard cells, cellulose reorganizes between a more homogenously distributed pattern in the open state and a more fibrillar, bundled pattern in the closed state. In the case of cellulose deficiency, stomatal aperture is larger because changes in guard cell length occur more readily. Cellulose reorganization is less evident, with more evenly spaced microfibrils in both open and closed states. In the absence of detectable xyloglucan, stomatal aperture is relatively smaller due to more restricted guard cell expansion and contraction, and cellulose is more bundled in both open and closed states. In *cesa7*$^{irx3-5}$ mutants, the overall size of the stomatal complex is smaller (Liang et al., 2010), but cellulose is not deficient in guard cells, with fibrillar patterns in both states. B, Conceptual model illustrating a possible scenario of how cellulose and xyloglucan in guard cell walls function in the regulation of stomatal aperture and cellulose reorganization.

facilitate repetitive wall expansion and contraction in response to reversible turgor pressure changes in guard cells during stomatal movements. In support of this idea, our results from imaging cellulose arrangement in the *cesa3*$^{je5}$ and *xxt1 xxt2* mutants, in relation to their stomatal phenotypes, show that both mutants display less evident cellulose reorganization, but in distinctive manners. *cesa3*$^{je5}$ guard cells have more diffuse S4B staining patterns in both open and closed states, and they also have larger stomatal apertures, possibly reflecting a reduced constraint on cell expansion. Previous S4B staining in *cesa6*$^{prc1\text{-}1}$ root cell walls revealed the presence of gaps in cellulose arrangement as a potential mechanism for their reduced anisotropic growth (Anderson et al., 2010). The distinct S4B staining patterns in *cesa3*$^{je5}$ guard cells versus *cesa6*$^{prc1\text{-}1}$ root cells might be due to different cell types or different reduction levels of cellulose content. *xxt1 xxt2* guard cells exhibit predominantly fibrillar patterns in both states, which matches the reduction in stomatal apertures (i.e. more constraints on expansion) and is consistent with previous S4B staining results in *xxt1 xxt2* root cells (Anderson et al., 2010). GFP-CESA3 expression in the *cesa3*$^{je5}$ mutant background restored cellulose reorganization in guard cells between the two functional states of stomata, but with overall higher anisotropy degrees than wild-type controls. A possible explanation is that the presence of the GFP tag on the CESA3 protein interferes with cellulose biosynthesis, disrupting cellulose microfibril formation and bundling. S4B staining in *cesa7*$^{irx3\text{-}5}$ guard cells revealed more anisotropic patterns in both open and closed states (Supplemental Fig. S14), which is not likely due to cellulose deficiency in guard cells, since S4B fluorescence intensity remained at wild-type levels in *cesa7*$^{irx3\text{-}5}$ guard cells. It is not known whether matrix wall polymers are altered or not in this mutant, but given that *cesa7*$^{irx3\text{-}5}$ guard cells are developmentally smaller (Liang et al., 2010), we hypothesize that such a loss of cellulose reorganization might be an indirect effect of deficient water supply on stomatal development.

Our observations of cellulose organization in guard cells by S4B staining, combined with stomatal aperture data, allow us to present interpretive schematics of cellulose and xyloglucan in guard cells during stomatal movements in different genotypes (Fig. 7A). We also present a conceptual model (Fig. 7B) to illustrate the relationships between our findings and other published results: guard cell expansion and contraction due to a sufficient amount of cellulose and xyloglucan present in guard cell walls (in the case of *cesa3*$^{je5}$ and *xxt1 xxt2*, respectively), and the size of an entire stomatal complex as a result of stomatal development (in the case of *cesa7*$^{irx3\text{-}5}$), contribute to the determination of stomatal aperture, influencing and/or influenced by cellulose reorganization between the two functional states of stomata. Given that *xxt1 xxt2* and *cesa7*$^{irx3\text{-}5}$ guard cells phenocopy each other in having more fibrillar S4B staining patterns, we speculate that cellulose reorganization might be more likely to depend on the proper control of stomatal complex size. It is also possible that the regulation of stomatal apertures and the dynamic changes of cellulose distribution in guard cells involve interactions between cellulose and xyloglucan, which are thought to take place at limited regions and are the targets of expansin action (Park and Cosgrove, 2012b; Cosgrove, 2014). In keeping with this idea, overexpression of the Arabidopsis $\alpha$-expansin gene *AtEXPA1* accelerates stomatal opening, likely by regulating the elastic properties of guard cell walls (Zhang et al., 2011). In general, we predict that modulating the mechanical properties of guard cell walls by altering wall synthesis, modification, or both will likely affect the dynamics and interactions of wall components and, thus, stomatal movements.

## CONCLUSION

In summary, we have observed short-term increases in nascent cellulose biosynthesis rates and a reduction in CESA particles colocalizing with MTs in guard cells as stomata close, suggesting a functional connection between the motility of CSCs and their association with MTs during stomatal movements in young tissues. By examining stomatal responses and the overall distribution patterns of existing cellulose in wild-type guard cells and in mutants deficient in cellulose or xyloglucan, we conclude that the regulation of normal guard cell length and stomatal aperture requires sufficient cellulose and xyloglucan production and is accompanied by the reorganization of cellulose from evenly spaced in the open state to bundled in the closed state. Future investigations of the structural details and the genetic underpinnings of guard cell wall composition, construction, modification, and dynamics will further advance our understanding of how these wall characteristics allow repetitive guard cell deformation as stomata open and close throughout the lifetime of the plant.

## MATERIALS AND METHODS

### Plant Materials, Growth Conditions, and Rosette Measurements

Arabidopsis (*Arabidopsis thaliana*) seeds of the Col-0 ecotype, the Col-2 ecotype (The Arabidopsis Biological Resource Center stock no. CS28170), the *cesa3*$^{je5}$ mutant (Desprez et al., 2007), the *cesa3*$^{eli1\text{-}1}$ mutant (Caño-Delgado et al., 2003), the *cesa6*$^{prc1\text{-}1}$ mutant (The Arabidopsis Biological Resource Center stock no. CS297; Desnos et al., 1996), the *cesa7*$^{irx3\text{-}5}$ mutant (Liang et al., 2010), the *xxt1 xxt2* mutant (The Arabidopsis Biological Resource Center stock no. CS16349; Cavalier et al., 2008), the transgenic line expressing GFP-CESA3 in the *cesa3*$^{je5}$ background (Desprez et al., 2007), the transgenic line expressing GFP-CESA1 in the *cesa1*$^{rsw1\text{-}10}$ background (Miart et al., 2014), the transgenic line expressing tdTomato-CESA6 in the *cesa6*$^{prc1\text{-}1}$ background (Sampathkumar et al., 2013), and the transgenic line expressing GFP-CESA3 and mCherry-TUA5 in the *cesa3*$^{je5}$ background (Gutierrez et al., 2009) were surface sterilized in 30% bleach with 0.1% SDS, washed four times with sterile water, suspended in 0.15% agar, and stratified at 4°C for at least 2 d. Seeds were sown on MS plates containing 2.2 g $L^{-1}$ MS salts (Caisson Laboratories), 0.6 g $L^{-1}$ MES, 1% (w/v) Suc, and 0.8% (w/v) agar, pH 5.6, and grown vertically at 22°C under 24 h of illumination. Ten-day-old seedlings were transferred from plates into soil supplemented with Miracle-Gro, and plants were grown in a chamber at 22°C with a 16-h-light/8-h-dark

photoperiod. Images of rosettes were captured with a Nikon D5100 DSLR camera, and rosette diameters were measured in ImageJ.

## *cesa3*$^{eli1\text{-}1}$ Genotyping

Genomic DNA of *cesa3*$^{eli1\text{-}1}$ mutants was isolated from 9-d-old seedlings using the Edwards method (Edwards et al., 1991). Forward primer 5′-ATTCCTTCATCACGGATCAATC-3′ and reverse primer 5′-AATCCTTTGAGTAATTGCTTCAG-3′ were used to amplify a 273-bp region that spans the *eli1-1* mutation site. The PCR product was then sequenced at the Huck Genomics Core Facility (Pennsylvania State University). Sequencing results revealed the previously reported C-to-T transition (Caño-Delgado et al., 2003), which leads to an amino acid substitution at position 291 (S291F) instead of 301 (S301F; Caño-Delgado et al., 2003). This disparity in mutation position is also reported in a more recent study (Pysh et al., 2012) and is likely due to updates in the Arabidopsis genome annotation (Lamesch et al., 2012).

## Confocal Microscopy and Image Analysis

All fluorescent confocal images of FP-CESA1/3/6 particles, GFP-CESA3 particle movement, colocalization between GFP-CESA3 and mCherry-TUA5, S4B staining, and CBM3a immunolabeling in guard cells were collected on a Zeiss Axio Observer microscope attached to a Yokogawa CSU-X1 spinning disk head with a 100× 1.4 numerical aperture immersion oil objective. All images were captured using the AxioVision 4.8 software (Carl Zeiss). A 488-nm excitation laser and a 525/50-nm emission filter were used for GFP; a 561-nm excitation laser was used for tdTomato, mCherry, and S4B, but with different band-pass emission filters (617/73 nm for tdTomato and S4B and 593/40 nm for mCherry).

Time-lapse images of GFP-CESA3 particle movement were recorded with an interval of 10 s and a duration of 5 min using 200-ms exposures. Image series were average projected in ImageJ to assess quality. To analyze GFP-CESA3 particle density in guard cells, the first or the second frame was extracted from a time-lapse image series as a substack. An ROI was defined by tracing the outline of a guard cell pair with the phenolic ester ring cropped. The area of the ROI was measured in ImageJ. GFP-CESA3 particles within the ROI were detected in Imaris 7.2 (Bitplane) with a 0.5-$\mu$m diameter. To analyze GFP-CESA3 particle speed, the same ROI was applied to the image series in ImageJ. The tracks that GFP-CESA3 particles move along were found in Imaris using the Connected Components algorithm with the minimum track duration set to 60 s. Displacement length and duration of the tracks were exported to calculate particle speed in nm min$^{-1}$. Analyses of GFP-CESA3 particle density and speed in surrounding pavement cells were performed using similar procedures.

Dual-channel z-series images of GFP-CESA3 and mCherry-TUA5 were obtained with a step size of 0.2 $\mu$m. To enhance the signal-to-noise ratio, images were first processed in ImageJ for background subtraction using the Sliding Paraboloid algorithm with a rolling ball radius of 30 pixels and for contrast enhancement with the saturated pixels set to 0.4%. To analyze the colocalization of GFP-CESA3 particles and mCherry-labeled MTs in guard cells, an ROI was defined in ImageJ by tracing the outline of a guard cell pair with the phenolic ester ring cropped out. GFP-CESA3 particles within the ROI were detected using the Spots tool in Imaris with a 0.5-$\mu$m estimated diameter. The total number of GFP-CESA3 particles detected was recorded, and the number of particles that colocalize with MTs was counted. The degree of colocalization between GFP-CESA3 particles and mCherry-TUA5 signal was determined as a percentage of the counts of colocalized particles over the total number of detected particles. To analyze the area and intensity of mCherry-TUA5-labeled MTs in guard cells, the same ROI was applied to the maximum projection of the original mCherry-TUA5 image in ImageJ, and guard cell area was recorded. Image thresholding and fluorescence quantification were performed as described previously (Kapp et al., 2015).

For S4B labeling of cellulose in guard cells, the abaxial sides of rosette leaves from 3- to 4-week-old plants were first gently abraded with carborundum powder (320 grit; Fisher Scientific) to disrupt the cuticle. Leaves were then inoculated with 0.1% (w/v) S4B (Anderson et al., 2010) in liquid MS medium using a 1-mL syringe (BD Luer-Lok) and stained for 30 min. Z-series images were obtained with a step size of 0.2 $\mu$m and the same settings of laser power, exposure time, and CCD gain value for all genotypes examined. To quantify S4B fluorescence intensity in guard cells, z-projections were generated in ImageJ using the Sum Slices algorithm, which converts images to 32-bit depth. Images were then converted back to 16-bit depth, and an ROI was defined by tracing the outline of a single guard cell. Raw integrated density (the sum of all pixel intensities within an ROI) and area were recorded. S4B fluorescence intensity was represented as a ratio of raw integrated density to area. Fluorescence intensity in guard cells from carborundum-abraded leaves without S4B staining was used as a control to subtract background fluorescence. To measure the anisotropy of S4B-stained cellulose, raw z-series images were analyzed in AutoQuant X2 (Media Cybernetics) for three-dimensional blind deconvolution. Maximum projections of the deconvolved z-series images were generated in ImageJ, and the anisotropy of S4B-stained cellulose microfibrils in guard cells was quantified using the FibrilTool plugin (Boudaoud et al., 2014) of ImageJ, with an ROI defined as half of a single guard cell bisected transversely. ANOVA tests were performed using the PAST statistics software package (Hammer et al., 2001) to compare S4B fluorescence intensity or anisotropy score among different genotypes or treatments.

For CBM3a immunolabeling of cellulose in guard cells, epidermis was peeled from the abaxial side of carborundum-abraded rosette leaves. Epidermal peels were first incubated with 10 $\mu$g mL$^{-1}$ CBM3a (PlantProbes, University of Leeds) in KPBST buffer (0.01 M $K_2HPO_4$, 0.5 M NaCl, and 0.1% Tween 20, pH 7.1) containing 3% (w/v) bovine serum albumin (BSA) for 24 h. Samples were then washed in KBPST buffer three times and incubated with a mouse anti-poly-His monoclonal antibody (Sigma) at a dilution of 1:100 in KBPST buffer containing 3% BSA for 8 h. After another three washing steps with KPBST buffer, samples were incubated with Alexa Fluor 488 goat anti-mouse IgG (Jackson ImmunoResearch) at a dilution of 1:100 in KBPST buffer containing 3% BSA for another 16 h in dark. Epidermal peels incubated with only Alexa Fluor 488 goat anti-mouse IgG under the same conditions were used as a negative control. After washing in KPBST buffer three times, z-stack images of the samples were collected with a step size of 0.2 $\mu$m and the same settings of laser power, exposure time, and CCD gain value for all genotypes examined. CBM3a immunolabeling fluorescence intensity was analyzed as described above for the quantification of S4B fluorescence intensity, except that only ROIs devoid of extremely bright signals were analyzed, because those signals came from regions that were severely damaged by carborundum abrasion, in which CBM3a and subsequent antibodies tended to accumulate.

## Stomatal Function Assays

For each mutant in every stomatal function assay, a Col-0 control grown under exactly the same conditions was used to correct any stomatal aperture changes caused by environmental variations. For stomatal closure assays, 6-d-old seedlings or rosette leaves from 3- to 4-week-old plants were first incubated in light for 2.5 h in a solution containing 20 mM KCl, 1 mM $CaCl_2$, and 5 mM MES-KOH, pH 6.15, to allow for stomatal opening. Stomatal closure was then induced by incubating the seedlings or leaves in the same solution in the dark or in the same solution with 50 $\mu$M ABA in the light for another 2.5 h. For stomatal opening assays, rosette leaves from 3- to 4-week-old plants were first incubated in the dark for 2.5 h in a solution containing 50 mM KCl, 0.1 mM $CaCl_2$, and 10 mM MES-KOH, pH 6.15, to allow for stomatal closure. Stomatal opening was then induced by incubating the leaves in the same solution in the light or in the same solution with 1 $\mu$M FC in the dark for another 2.5 h. To measure stomatal apertures in 6-d-old seedlings, 100 $\mu$g mL$^{-1}$ PI (Life Technologies; catalog no. P3566) was used to stain cell outlines 5 min before imaging. Snapshot images of PI-stained stomatal guard cells were collected on a spinning disk confocal microscope using a 561-nm excitation laser and a 617/73-nm emission filter with a 63× 1.4 numerical aperture immersion oil objective. For rosette leaves, the epidermis was peeled from the abaxial side, and snapshot images were taken on the confocal microscope under bright-field light with the 63× objective. Stomatal pore dimensions (aperture and pore length), guard cell pair dimensions (guard cell pair height and guard cell pair width), and guard cell dimensions (guard cell diameter and guard cell length) were measured using ImageJ.

## Cellulase and DCB Treatments

Cellulase (CEG, from *Aspergillus niger*; Park and Cosgrove, 2012b) was a kind gift from Xuan Wang (Dr. Daniel Cosgrove's laboratory, Pennsylvania State University) and was originally purchased from Megazyme. Epidermal peels from the abaxial side of 3-week-old Col-0 rosette leaves were first incubated with 10 units mL$^{-1}$ CEG in 10 mM MES, pH 4.5, at 30°C in the dark for 1 h, then transferred to a solution containing 50 mM KCl, 0.1 mM $CaCl_2$, and 10 mM MES-KOH, pH 6.15, at room temperature in the dark for 2.5 h, and induced to open in the same solution with 1 $\mu$M FC at room temperature in the dark for another 2.5 h. Snapshot images of stomata were taken on the confocal microscope under bright-field light with the 63× objective.

DCB (Chem Service; DeBolt et al., 2007) was applied to 6-d-old Col-0 seedlings at 10 $\mu$M in a solution containing 50 mM KCl, 0.1 mM $CaCl_2$, and 10 mM MES-KOH, pH 6.15, at room temperature in the dark for 2.5 h. Stomatal opening was then induced by incubating seedlings with 1 $\mu$M FC in the same solution without DCB at room temperature in the dark for another 2.5 h. Seedlings were stained with 100 $\mu$g $mL^{-1}$ PI for 5 min, and snapshot images of stomata were obtained on the confocal microscope with the 561-nm excitation laser and the 617/73-nm emission filter with the 63× objective. To verify the effect of DCB on inhibiting CSC motility at the plasma membrane, DCB was also applied to 6-d-old transgenic seedlings expressing GFP-CESA3 at the same concentration under the same conditions for 2.5 h, and time-lapse images of GFP-CESA3 were recorded with an interval of 10 s and a duration of 5 min.

## Cellulose Content Measurements

Cellulose contents were measured following the Updegraff method (Updegraff, 1969). Twenty-three-day-old Col-0, *cesa3$^{je5}$*, *GFP-CESA3*, *cesa3$^{eli1-1}$*, and *cesa6$^{prc1-1}$* plants grown under a 16-h-light/8-h-dark regime at 22°C were placed in the dark for 24 h before harvesting. Rosette leaves of each genotype were first incubated in 80% ethanol overnight at 65°C. After removal of ethanol, samples were incubated in acetone at room temperature overnight and then allowed to air dry in a chemical fume hood for 4 d. Dried samples were ball milled into powder using a Restch Cryomill at room temperature for 5 min. The powder was weighed, added to 2-mL screw-cap polypropylene tubes, and boiled in a solution containing acetic acid:nitric acid:water (8:2:1) for 30 min. After centrifuging for 5 min at 21,130*g*, the pellets were resuspended in 1 mL of 67% sulfuric acid. Fifty microliters of the resuspended sample was added into a 10-mL screw-cap glass tube, 1 mL of 0.2% anthrone in concentrated sulfuric acid was added to each sample, and $A_{620}$ was recorded on a NanoDrop 2000C spectrophotometer (Thermo Scientific).

Sequence data from this article can be found in the Arabidopsis Genome Initiative or GenBank/EMBL databases under the following accession numbers: *CESA1* (At4g32410), *CESA3* (At5g05170), *CESA6* (At5g64740), *CESA7* (At5g17420), *TUA5* (At5g19780), *XXT1* (At3g62720), and *XXT2* (At4g02500).

## Supplemental Data

The following supplemental materials are available.

**Supplemental Figure S1.** Distributions of FP-CESA particles in guard cells from cotyledons at different ages.

**Supplemental Figure S2.** Stomata in young seedlings respond to stimuli that induce stomatal opening or closure.

**Supplemental Figure S3.** GFP-CESA3 particles in neighboring pavement cells have faster movement after 50 $\mu$M ABA treatment for 2.5 h.

**Supplemental Figure S4.** GFP-CESA3 particle speed is increased in neighboring pavement cells after dark treatment for 2.5 h.

**Supplemental Figure S5.** Colocalization analysis of GFP-CESA3 particles and MTs in neighboring pavement cells.

**Supplemental Figure S6.** Legend of measurements in a stomatal complex.

**Supplemental Figure S7.** Representative images of S4B staining and CBM3a immunolabeling in guard cells of Col-0, *cesa3$^{je5}$*, *cesa3$^{eli1-1}$*, and *cesa6$^{prc1-1}$* plants.

**Supplemental Figure S8.** Stomatal patterning phenotype in *cesa3$^{je5}$* mutants.

**Supplemental Figure S9.** Rosette leaf phenotype and measurement of guard cell diameter and length in Col-0 and *cesa3$^{je5}$* plants.

**Supplemental Figure S10.** Rosette leaf phenotype and measurement of guard cell diameter and length in Col-0 and GFP-CESA3 plants.

**Supplemental Figure S11.** Stomatal responses to FC after cellulase or DCB treatment.

**Supplemental Figure S12.** Stomatal patterning, rosette leaf phenotype, and measurement of guard cell diameter and length in Col-0 and *xxt1 xxt2* plants.

**Supplemental Figure S13.** S4B-stained cellulose distribution patterns and anisotropy measurements in open versus closed stomatal guard cells induced by light or dark treatment in Col-0, *cesa3$^{eli1-1}$*, and *cesa6$^{prc1-1}$* plants.

**Supplemental Figure S14.** S4B-stained cellulose distribution patterns and anisotropy measurements in open versus closed stomatal guard cells of Col-2 and *cesa7$^{irx3-5}$* plants.

**Supplemental Table S1.** Measurement of GFP-CESA3 particle density in guard cells, guard cell area, the ratio of thresholded area to guard cell area, and fluorescence intensity of mCherry-TUA5-labeled MTs in guard cells under the light control condition or after dark treatment for 30 min.

**Supplemental Movie S1.** GFP-CESA3 particle dynamics at the plasma membrane in guard cells in the absence of ABA.

**Supplemental Movie S2.** GFP-CESA3 particle dynamics at the plasma membrane in guard cells after 50 $\mu$M ABA treatment for 2.5 h.

**Supplemental Movie S3.** GFP-CESA3 particle dynamics at the plasma membrane in guard cells under the light control condition.

**Supplemental Movie S4.** GFP-CESA3 particle dynamics at the plasma membrane in guard cells after dark treatment for 2.5 h.

## ACKNOWLEDGMENTS

We thank Dr. Sarah M. Assmann for insightful comments on the article, Dr. Chaowen Xiao for technical assistance with cellulose content measurements, Xuan Wang and Dr. Daniel Cosgrove for providing the cellulase used in this work, Devon Fischer for performing stomatal aperture measurements in *cesa3$^{eli1-1}$* and *cesa6$^{prc1-1}$* mutants, Igor Andrzhievsky and Melissa Ishler for assistance with guard cell dimension measurements, Missy Hazen for assistance with image deconvolution, Dr. Shaolin Chen for providing *cesa3$^{je5}$* seeds, Dr. Joseph Hill, Jr., for providing *cesa3$^{eli1-1}$* seeds, Dr. Kian Hematy for providing *cesa6$^{prc1-1}$* seeds and GFP-CESA3 transgenic seeds, Dr. Samantha Vernhettes for providing GFP-CESA1 transgenic seeds, Dr. Staffan Persson for providing tdTomato-CESA6 transgenic seeds, Dr. David Ehrhardt for providing GFP-CESA3; mCherry-TUA5 double-labeled lines, and Dr. Alistair Hetherington for providing Col-2 and *cesa7$^{irx3-5}$* seeds.

Received July 8, 2015; accepted January 3, 2016; published January 4, 2016.

## LITERATURE CITED

**Anderson CT, Carroll A, Akhmetova L, Somerville C** (2010) Real-time imaging of cellulose reorientation during cell wall expansion in Arabidopsis roots. Plant Physiol **152:** 787–796

**Arioli T, Peng L, Betzner AS, Burn J, Wittke W, Herth W, Camilleri C, Höfte H, Plazinski J, Birch R, et al** (1998) Molecular analysis of cellulose biosynthesis in Arabidopsis. Science **279:** 717–720

**Baskin TI** (2005) Anisotropic expansion of the plant cell wall. Annu Rev Cell Dev Biol **21:** 203–222

**Bates GW, Rosenthal DM, Sun J, Chattopadhyay M, Peffer E, Yang J, Ort DR, Jones AM** (2012) A comparative study of the Arabidopsis thaliana guard-cell transcriptome and its modulation by sucrose. PLoS ONE **7:** e49641

**Bergmann DC, Sack FD** (2007) Stomatal development. Annu Rev Plant Biol **58:** 163–181

**Bischoff V, Desprez T, Mouille G, Vernhettes S, Gonneau M, Höfte H** (2011) Phytochrome regulation of cellulose synthesis in Arabidopsis. Curr Biol **21:** 1822–1827

**Blake AW, McCartney L, Flint JE, Bolam DN, Boraston AB, Gilbert HJ, Knox JP** (2006) Understanding the biological rationale for the diversity of cellulose-directed carbohydrate-binding modules in prokaryotic enzymes. J Biol Chem **281:** 29321–29329

**Boex-Fontvieille E, Davanture M, Jossier M, Zivy M, Hodges M, Tcherkez G** (2014) Photosynthetic activity influences cellulose biosynthesis and phosphorylation of proteins involved therein in Arabidopsis leaves. J Exp Bot **65:** 4997–5010

**Boudaoud A, Burian A, Borowska-Wykręt D, Uyttewaal M, Wrzalik R, Kwiatkowska D, Hamant O** (2014) FibrilTool, an ImageJ plug-in to quantify fibrillar structures in raw microscopy images. Nat Protoc **9:** 457–463

**Caño-Delgado A, Penfield S, Smith C, Catley M, Bevan M** (2003) Reduced cellulose synthesis invokes lignification and defense responses in Arabidopsis thaliana. Plant J **34:** 351–362

**Casson SA, Hetherington AM** (2010) Environmental regulation of stomatal development. Curr Opin Plant Biol **13:** 90–95

**Cavalier DM, Lerouxel O, Neumetzler L, Yamauchi K, Reinecke A, Freshour G, Zabotina OA, Hahn MG, Burgert I, Pauly M, et al** (2008) Disrupting two Arabidopsis thaliana xylosyltransferase genes results in plants deficient in xyloglucan, a major primary cell wall component. Plant Cell **20:** 1519–1537

**Chen S, Ehrhardt DW, Somerville CR** (2010) Mutations of cellulose synthase (CESA1) phosphorylation sites modulate anisotropic cell expansion and bidirectional mobility of cellulose synthase. Proc Natl Acad Sci USA **107:** 17188–17193

**Cosgrove DJ** (2005) Growth of the plant cell wall. Nat Rev Mol Cell Biol **6:** 850–861

**Cosgrove DJ** (2014) Re-constructing our models of cellulose and primary cell wall assembly. Curr Opin Plant Biol **22:** 122–131

**DeBolt S, Gutierrez R, Ehrhardt DW, Somerville C** (2007) Nonmotile cellulose synthase subunits repeatedly accumulate within localized regions at the plasma membrane in Arabidopsis hypocotyl cells following 2,6-dichlorobenzonitrile treatment. Plant Physiol **145:** 334–338

**Desnos T, Orbović V, Bellini C, Kronenberger J, Caboche M, Traas J, Höfte H** (1996) Procuste1 mutants identify two distinct genetic pathways controlling hypocotyl cell elongation, respectively in dark- and light-grown Arabidopsis seedlings. Development **122:** 683–693

**Desprez T, Juraniec M, Crowell EF, Jouy H, Pochylova Z, Parcy F, Höfte H, Gonneau M, Vernhettes S** (2007) Organization of cellulose synthase complexes involved in primary cell wall synthesis in Arabidopsis thaliana. Proc Natl Acad Sci USA **104:** 15572–15577

**Edwards K, Johnstone C, Thompson C** (1991) A simple and rapid method for the preparation of plant genomic DNA for PCR analysis. Nucleic Acids Res **19:** 1349

**Eisinger W, Ehrhardt D, Briggs W** (2012a) Microtubules are essential for guard-cell function in Vicia and Arabidopsis. Mol Plant **5:** 601–610

**Eisinger WR, Kirik V, Lewis C, Ehrhardt DW, Briggs WR** (2012b) Quantitative changes in microtubule distribution correlate with guard cell function in Arabidopsis. Mol Plant **5:** 716–725

**Fagard M, Desnos T, Desprez T, Goubet F, Refregier G, Mouille G, McCann M, Rayon C, Vernhettes S, Höfte H** (2000) PROCUSTE1 encodes a cellulose synthase required for normal cell elongation specifically in roots and dark-grown hypocotyls of *Arabidopsis*. Plant Cell **12:** 2409–2424

**Feraru E, Feraru MI, Kleine-Vehn J, Martinière A, Mouille G, Vanneste S, Vernhettes S, Runions J, Friml J** (2011) PIN polarity maintenance by the cell wall in Arabidopsis. Curr Biol **21:** 338–343

**Franks PJ, Buckley TN, Shope JC, Mott KA** (2001) Guard cell volume and pressure measured concurrently by confocal microscopy and the cell pressure probe. Plant Physiol **125:** 1577–1584

**Franks PJ, Cowan IR, Farquhar GD** (1998) A study of stomatal mechanics using the cell pressure probe. Plant Cell Environ **21:** 94–100

**Fujita M, Himmelspach R, Hocart CH, Williamson RE, Mansfield SD, Wasteneys GO** (2011) Cortical microtubules optimize cell-wall crystallinity to drive unidirectional growth in Arabidopsis. Plant J **66:** 915–928

**Fujita M, Wasteneys GO** (2014) A survey of cellulose microfibril patterns in dividing, expanding, and differentiating cells of Arabidopsis thaliana. Protoplasma **251:** 687–698

**Green PB** (1962) Mechanism for plant cellular morphogenesis. Science **138:** 1404–1405

**Griffiths JS, Šola K, Kushwaha R, Lam P, Tateno M, Young R, Voiniciuc C, Dean G, Mansfield SD, DeBolt S, et al** (2015) Unidirectional movement of cellulose synthase complexes in Arabidopsis seed coat epidermal cells deposit cellulose involved in mucilage extrusion, adherence, and ray formation. Plant Physiol **168:** 502–520

**Gu Y, Kaplinsky N, Bringmann M, Cobb A, Carroll A, Sampathkumar A, Baskin TI, Persson S, Somerville CR** (2010) Identification of a cellulose synthase-associated protein required for cellulose biosynthesis. Proc Natl Acad Sci USA **107:** 12866–12871

**Gutierrez R, Lindeboom JJ, Paredez AR, Emons AM, Ehrhardt DW** (2009) Arabidopsis cortical microtubules position cellulose synthase delivery to the plasma membrane and interact with cellulose synthase trafficking compartments. Nat Cell Biol **11:** 797–806

**Hammer Ø, Harper DAT, Ryan PD** (2001) PAST: paleontological statistics software package for education and data analysis. Palaeontol Electronica **4:** 1–9

**Hématy K, Sado PE, Van Tuinen A, Rochange S, Desnos T, Balzergue S, Pelletier S, Renou JP, Höfte H** (2007) A receptor-like kinase mediates the response of Arabidopsis cells to the inhibition of cellulose synthesis. Curr Biol **17:** 922–931

**Jones L, Milne JL, Ashford D, McCann MC, McQueen-Mason SJ** (2005) A conserved functional role of pectic polymers in stomatal guard cells from a range of plant species. Planta **221:** 255–264

**Jones L, Milne JL, Ashford D, McQueen-Mason SJ** (2003) Cell wall arabinan is essential for guard cell function. Proc Natl Acad Sci USA **100:** 11783–11788

**Kapp N, Barnes WJ, Richard TL, Anderson CT** (2015) Imaging with the fluorogenic dye Basic Fuchsin reveals subcellular patterning and ecotype variation of lignification in Brachypodium distachyon. J Exp Bot **66:** 4295–4304

**Kim TH, Böhmer M, Hu H, Nishimura N, Schroeder JI** (2010) Guard cell signal transduction network: advances in understanding abscisic acid, $CO_2$, and $Ca^{2+}$ signaling. Annu Rev Plant Biol **61:** 561–591

**Kimura S, Laosinchai W, Itoh T, Cui X, Linder CR, Brown RM Jr** (1999) Immunogold labeling of rosette terminal cellulose-synthesizing complexes in the vascular plant *Vigna angularis*. Plant Cell **11:** 2075–2086

**Kollist H, Nuhkat M, Roelfsema MR** (2014) Closing gaps: linking elements that control stomatal movement. New Phytol **203:** 44–62

**Kong D, Karve R, Willet A, Chen MK, Oden J, Shpak ED** (2012) Regulation of plasmodesmatal permeability and stomatal patterning by the glycosyltransferase-like protein KOBITO1. Plant Physiol **159:** 156–168

**Lake JA, Woodward FI** (2008) Response of stomatal numbers to $CO_2$ and humidity: control by transpiration rate and abscisic acid. New Phytol **179:** 397–404

**Lamesch P, Berardini TZ, Li D, Swarbreck D, Wilks C, Sasidharan R, Muller R, Dreher K, Alexander DL, Garcia-Hernandez M, et al** (2012) The Arabidopsis Information Resource (TAIR): improved gene annotation and new tools. Nucleic Acids Res **40:** D1202–D1210

**Larkin JC, Marks MD, Nadeau J, Sack F** (1997) Epidermal cell fate and patterning in leaves. Plant Cell **9:** 1109–1120

**Lei L, Li S, Du J, Bashline L, Gu Y** (2013) Cellulose synthase INTERACTIVE3 regulates cellulose biosynthesis in both a microtubule-dependent and microtubule-independent manner in *Arabidopsis*. Plant Cell **25:** 4912–4923

**Li B, Liu G, Deng Y, Xie M, Feng Z, Sun M, Zhao Y, Liang L, Ding N, Jia W** (2010) Excretion and folding of plasmalemma function to accommodate alterations in guard cell volume during stomatal closure in Vicia faba L. J Exp Bot **61:** 3749–3758

**Li S, Lei L, Somerville CR, Gu Y** (2012) Cellulose synthase interactive protein 1 (CSI1) links microtubules and cellulose synthase complexes. Proc Natl Acad Sci USA **109:** 185–190

**Liang YK, Xie X, Lindsay SE, Wang YB, Masle J, Williamson L, Leyser O, Hetherington AM** (2010) Cell wall composition contributes to the control of transpiration efficiency in Arabidopsis thaliana. Plant J **64:** 679–686

**Lucas JR, Nadeau JA, Sack FD** (2006) Microtubule arrays and Arabidopsis stomatal development. J Exp Bot **57:** 71–79

**MacKinnon IM, Sturcová A, Sugimoto-Shirasu K, His I, McCann MC, Jarvis MC** (2006) Cell-wall structure and anisotropy in procuste, a cellulose synthase mutant of Arabidopsis thaliana. Planta **224:** 438–448

**Majewska-Sawka A, Münster A, Rodríguez-García MI** (2002) Guard cell wall: immunocytochemical detection of polysaccharide components. J Exp Bot **53:** 1067–1079

**McFarlane HE, Döring A, Persson S** (2014) The cell biology of cellulose synthesis. Annu Rev Plant Biol **65:** 69–94

**Meckel T, Gall L, Semrau S, Homann U, Thiel G** (2007) Guard cells elongate: relationship of volume and surface area during stomatal movement. Biophys J **92:** 1072–1080

**Miart F, Desprez T, Biot E, Morin H, Belcram K, Hofte H, Gonneau M, Vernhettes S** (2014) Spatio-temporal analysis of cellulose synthesis during cell plate formation in Arabidopsis. Plant J **77:** 71–84

**Palevitz BA, Hepler PK** (1976) Cellulose microfibril orientation and cell shaping in developing guard cells of Allium: the role of microtubules and ion accumulation. Planta **132:** 71–93

**Paredez AR, Somerville CR, Ehrhardt DW** (2006) Visualization of cellulose synthase demonstrates functional association with microtubules. Science **312:** 1491–1495

**Park YB, Cosgrove DJ** (2012a) Changes in cell wall biomechanical properties in the xyloglucan-deficient *xxt1/xxt2* mutant of Arabidopsis. Plant Physiol **158:** 465–475

**Park YB, Cosgrove DJ** (2012b) A revised architecture of primary cell walls based on biomechanical changes induced by substrate-specific endoglucanases. Plant Physiol **158:** 1933–1943

**Persson S, Paredez A, Carroll A, Palsdottir H, Doblin M, Poindexter P, Khitrov N, Auer M, Somerville CR** (2007) Genetic evidence for three unique components in primary cell-wall cellulose synthase complexes in Arabidopsis. Proc Natl Acad Sci USA **104:** 15566–15571

**Pillitteri LJ, Torii KU** (2012) Mechanisms of stomatal development. Annu Rev Plant Biol **63:** 591–614

**Pysh L, Alexander N, Swatzyna L, Harbert R** (2012) Four alleles of AtCESA3 form an allelic series with respect to root phenotype in Arabidopsis thaliana. Physiol Plant **144:** 369–381

**Richmond T** (2000) Higher plant cellulose synthases. Genome Biol **1:** S3001

**Sampathkumar A, Gutierrez R, McFarlane HE, Bringmann M, Lindeboom J, Emons AM, Samuels L, Ketelaar T, Ehrhardt DW, Persson S** (2013) Patterning and lifetime of plasma membrane-localized cellulose synthase is dependent on actin organization in Arabidopsis interphase cells. Plant Physiol **162:** 675–688

**Scheible WR, Eshed R, Richmond T, Delmer D, Somerville C** (2001) Modifications of cellulose synthase confer resistance to isoxaben and thiazolidinone herbicides in Arabidopsis Ixr1 mutants. Proc Natl Acad Sci USA **98:** 10079–10084

**Shope JC, DeWald DB, Mott KA** (2003) Changes in surface area of intact guard cells are correlated with membrane internalization. Plant Physiol **133:** 1314–1321

**Somerville C** (2006) Cellulose synthesis in higher plants. Annu Rev Cell Dev Biol **22:** 53–78

**Somerville C, Bauer S, Brininstool G, Facette M, Hamann T, Milne J, Osborne E, Paredez A, Persson S, Raab T, et al** (2004) Toward a systems approach to understanding plant cell walls. Science **306:** 2206–2211

**Taylor NG, Howells RM, Huttly AK, Vickers K, Turner SR** (2003) Interactions among three distinct CesA proteins essential for cellulose synthesis. Proc Natl Acad Sci USA **100:** 1450–1455

**Taylor NG, Scheible WR, Cutler S, Somerville CR, Turner SR** (1999) The *irregular xylem3* locus of *Arabidopsis* encodes a cellulose synthase required for secondary cell wall synthesis. Plant Cell **11:** 769–780

**Tormo J, Lamed R, Chirino AJ, Morag E, Bayer EA, Shoham Y, Steitz TA** (1996) Crystal structure of a bacterial family-III cellulose-binding domain: a general mechanism for attachment to cellulose. EMBO J **15:** 5739–5751

**Turner SR, Somerville CR** (1997) Collapsed xylem phenotype of *Arabidopsis* identifies mutants deficient in cellulose deposition in the secondary cell wall. Plant Cell **9:** 689–701

**Updegraff DM** (1969) Semimicro determination of cellulose in biological materials. Anal Biochem **32:** 420–424

**Wolf S, Hématy K, Höfte H** (2012) Growth control and cell wall signaling in plants. Annu Rev Plant Biol **63:** 381–407

**Wu H, Sharpe PJH, Spence RD** (1985) Stomatal mechanics. III. Geometric interpretation of the mechanical advantage. Plant Cell Environ **8:** 269–274

**Xiao C, Zhang T, Zheng Y, Cosgrove DJ, Anderson CT** (2016) Xyloglucan deficiency disrupts microtubule stability and cellulose biosynthesis in Arabidopsis, altering cell growth and morphogenesis. Plant Physiol **170:** 234–249

**Yang Y, Costa A, Leonhardt N, Siegel RS, Schroeder JI** (2008) Isolation of a strong Arabidopsis guard cell promoter and its potential as a research tool. Plant Methods **4:** 6

**Zablackis E, Huang J, Müller B, Darvill AG, Albersheim P** (1995) Characterization of the cell-wall polysaccharides of Arabidopsis thaliana leaves. Plant Physiol **107:** 1129–1138

**Zeiger E** (1983) The biology of stomatal guard cells. Annu Rev Plant Physiol **34:** 441–475

**Zhang XQ, Wei PC, Xiong YM, Yang Y, Chen J, Wang XC** (2011) Overexpression of the Arabidopsis $\alpha$-expansin gene AtEXPA1 accelerates stomatal opening by decreasing the volumetric elastic modulus. Plant Cell Rep **30:** 27–36

**Zhong R, Lee C, Ye ZH** (2010) Evolutionary conservation of the transcriptional network regulating secondary cell wall biosynthesis. Trends Plant Sci **15:** 625–632